FUS inclusions disrupt RNA localization by sequestering kinesin-1 and inhibiting microtubule detyrosination

Kyota Yasuda,[1] Sarah F. Clatterbuck-Soper,[1] Meredith E. Jackrel,[2] James Shorter,[2] and Stavroula Mili[1]

[1]Laboratory of Cellular and Molecular Biology, Center for Cancer Research, National Cancer Institute, National Institutes of Health, Bethesda, MD 20892
[2]Department of Biochemistry and Biophysics, Perelman School of Medicine at the University of Pennsylvania, Philadelphia, PA 19104

Cytoplasmic inclusions of the RNA-binding protein fused in sarcoma (FUS) represent one type of membraneless ribonucleoprotein compartment. Formation of FUS inclusions is promoted by amyotrophic lateral sclerosis (ALS)–linked mutations, but the cellular functions affected upon inclusion formation are poorly defined. In this study, we find that FUS inclusions lead to the mislocalization of specific RNAs from fibroblast cell protrusions and neuronal axons. This is mediated by recruitment of kinesin-1 mRNA and protein within FUS inclusions, leading to a loss of detyrosinated glutamate (Glu)–microtubules (MTs; Glu-MTs) and an inability to support the localization of RNAs at protrusions. Importantly, dissolution of FUS inclusions using engineered Hsp104 disaggregases, or overexpression of kinesin-1, reverses these effects. We further provide evidence that kinesin-1 affects MT detyrosination not through changes in MT stability, but rather through targeting the tubulin carboxypeptidase enzyme onto specific MTs. Interestingly, other pathological inclusions lead to similar outcomes, but through apparently distinct mechanisms. These results reveal a novel kinesin-dependent mechanism controlling the MT cytoskeleton and identify loss of Glu-MTs and RNA mislocalization as common outcomes of ALS pathogenic mutations.

Introduction

RNA-binding proteins with low-complexity domains (LCDs) are central in compartmentalizing the nuclear and cytoplasmic environments. LCD-containing proteins drive the formation of membraneless inclusions, such as stress granules and P-bodies, through a process of liquid–liquid phase separation (Weber and Brangwynne, 2012; Courchaine et al., 2016; Protter and Parker, 2016). The LCD-containing protein FUS (fused in sarcoma; also known as translocated in liposarcoma [TLS]) is mutated in amyotrophic lateral sclerosis (ALS), and a hallmark of ALS-FUS patients is the formation of FUS inclusions (Blokhuis et al., 2013; Li et al., 2013; Ling et al., 2013; Shelkovnikova, 2013).

Evidence from model systems suggests that inclusion formation is causatively related to disease. In yeast, FUS aggregation in the cytoplasm induces toxicity (Sun et al., 2011). In *Caenorhabditis elegans*, the abundance of insoluble FUS directly correlates with neurotoxicity, and promoting or reducing FUS aggregation enhances or ameliorates disease phenotypes, respectively (Murakami et al., 2015). Furthermore, aggregate dissolution can have beneficial effects. Hsp104, a hexameric AAA+ ATPase that deconstructs amyloid fibrils, preamyloid oligomers, and disordered aggregates, has been engineered to target pathological aggregates for dissolution. Engineered Hsp104 variants dissolve FUS aggregates in yeast and suppress FUS toxicity (Jackrel and Shorter, 2014; Jackrel et al., 2014).

ALS mutations in FUS have been mapped to both coding and noncoding regions. Most coding mutations cluster at a C-terminal NLS and disrupt its activity (Dormann et al., 2010; Lagier-Tourenne et al., 2010; Renton et al., 2014). Mutant FUS proteins accumulate at higher levels in the cytoplasm and promote the formation of inclusions that also contain marker proteins commonly associated with stress granules (Li et al., 2013; Ramaswami et al., 2013). Disease mutations have additionally been found in the FUS 3′UTR and have been shown to increase its abundance and disrupt its regulation by miRNAs (Sabatelli et al., 2013; Dini Modigliani et al., 2014). Consistently, FUS inclusions can form either preferentially upon stress or spontaneously upon overexpression. Moreover, wild-type FUS is frequently found to be aggregated in the cytoplasm of degenerating neurons in a significant fraction of cases of frontotemporal dementia, termed FTD-FUS (Ling et al., 2013).

FUS inclusions have been proposed to exert pathogenic effects either through preventing normal FUS functions in the nucleus or cytoplasm or through exerting a toxic gain of function (for example, through sequestering other protein factors;

Correspondence to Stavroula Mili: voula.mili@nih.gov

Abbreviations used: ALS, amyotrophic lateral sclerosis; APC, adenomatous polyposis coli; DIV, day in vitro; IDR, intrinsically disordered region; IF, immunofluorescence; LCD, low-complexity domain; MT, microtubule; TCP, tubulin carboxypeptidase; TTL, tubulin-tyrosine ligase; WB, Western blot.

The Rockefeller University Press $30.00
J. Cell Biol. Vol. 216 No. 4 1015–1034
https://doi.org/10.1083/jcb.201608022

Blokhuis et al., 2013; Ling et al., 2013; Ramaswami et al., 2013; Murakami et al., 2015). FUS binds to thousands of RNA targets through loosely defined consensus sequences (Hoell et al., 2011; Ishigaki et al., 2012; Rogelj et al., 2012; Nakaya et al., 2013) and has been assigned several roles, including transcription regulation, miRNA processing, mRNA splicing, mRNA stability, and transport (Tan and Manley, 2009; Lagier-Tourenne et al., 2010; Ling et al., 2013). However, whether these or other effects are relevant to the pathogenic process is not known.

We had previously shown that wild-type FUS associates with and regulates the translation of RNAs localized at protrusive areas of cells (Yasuda et al., 2013). These RNAs require the adenomatous polyposis coli (APC) tumor-suppressor protein for their localization (thus they are hereafter termed APC-dependent RNAs) and are anchored at the plus ends of Glu-microtubules (MTs [Glu-MTs]; Mili et al., 2008). Glu-MTs are generated by an unknown tubulin carboxypeptidase (TCP), which removes the C-terminal tyrosine of α-tubulin to expose a Glu residue (Hammond et al., 2008; Janke, 2014). Glu-MTs can be preferentially recognized by MT motors and are required for specific functions during interphase and mitosis (Dunn et al., 2008; Cai et al., 2009; Konishi and Setou, 2009; Barisic et al., 2015; Herms et al., 2015).

In this study, we reveal a new mechanism affected by the formation of FUS inclusions. We investigated how the formation of cytoplasmic inclusions by ALS-associated FUS mutants affects APC-dependent RNA localization. We found that the formation of cytoplasmic FUS inclusions is required for the mislocalization of RNAs from cell protrusions. The underlying mechanism involves the recruitment of kinesin-1 mRNA and protein within inclusions, leading to a loss of Glu-MTs and an inability to support transport and/or anchoring of APC-dependent RNAs. We further investigated the mechanism through which kinesin-1 affects MT detyrosination, and we offer evidence that it does not involve changes in MT stability but rather relies on the ability of kinesin-1 to target the TCP enzyme onto specific MTs. Interestingly, loss of Glu-MTs and RNA mislocalization are also observed in the presence of other disease-associated inclusions, such as those formed by mutant TDP-43. However, in this case, the underlying mechanisms appear to be distinct. Overall, these results reveal a novel kinesin-dependent mechanism controlling the MT cytoskeleton, which is disrupted by ALS pathogenic mutations and leads to the disruption of RNA localization.

Results

Cytoplasmic FUS inclusions do not affect overall cellular architecture or induce stress response markers

We set out to investigate how ALS-associated FUS mutants impact the localization of APC-dependent RNAs. As described previously (Kwiatkowski et al., 2009; Bosco et al., 2010; Vance et al., 2013), exogenously expressed FUS mutants carrying NLS mutations form inclusions in the cytoplasm of a fraction of fibroblast cells (we refer to these interchangeably as inclusions or granules throughout the text). At equivalent expression levels, the frequency of inclusion formation correlates with the severity of disease outcome associated with each particular mutation (10–15% of inclusion-containing cells for GFP-FUS(R521C) and 40–50% for GFP-FUS(R495X) and GFP-FUS(P525L)). The coding ALS mutations provide only one way of promoting FUS inclusion formation. Consistent with the fact that pathogenic mutations are also found in noncoding regions of the FUS gene and increase FUS protein abundance (see Introduction), overexpression of the wild-type protein can similarly induce the formation of inclusions (albeit in fewer cells compared with cells expressing equivalent amounts of mutant FUS proteins; Yasuda et al., 2013).

Cytoplasmic FUS-induced inclusions recruit markers of stress granules, such as the proteins TIA-1 and FMRP, as we have described previously (Yasuda et al., 2013). Furthermore, these structures likely correspond to liquid droplet–like structures (Baron et al., 2013; Patel et al., 2015) because FRAP experiments indicate that, to a significant extent, there is a dynamic exchange of mutant GFP-FUS found within inclusions with the free cytoplasmic pool (Fig. S1 A). However, despite the similarity to stress granules, formation of FUS inclusions was not accompanied by the induction of a stress response, indicated by the lack of an increase in phopsho-eIF2α levels both in Western blot (WB) and immunofluorescence (IF) experiments (Fig. S1, B and C). Nevertheless, phospho-eIF2α was induced to similar levels in both control and FUS inclusion–containing cells upon treatment with sodium arsenite (Fig. S1 C). Furthermore, the presence of FUS inclusions did not induce the unfolded protein response, as indicated by the lack of accumulation of the spliced form of *XBP1* mRNA (Fig. S1, D and E), and also did not detectably affect the overall cellular architecture, as assessed by the distribution of mitochondria, Golgi, and ER (Fig. S1 F).

Formation of cytoplasmic FUS inclusions leads to a specific mislocalization of RNAs from cell protrusions

To quantitatively assess any effects on RNA localization at cell protrusions, we imaged cells plated on Y-shaped micropatterned substrates to limit any effects caused by differences in cell shape (Fig. 1 A). A peripheral RNA localization metric, termed the "edge ratio," was calculated as the fraction of RNA found within a specified distance from the outside cell boundary normalized to the corresponding area (Fig. 1 A). This metric clearly distinguishes diffusely distributed RNAs from peripherally enriched RNAs and provides an overview of peripheral RNA accumulation within a population of cells. The *Ddr2* RNA, encoding a discoidin domain collagen receptor, was used as a representative APC-dependent localized RNA (Mili et al., 2008; Yasuda et al., 2013). We have observed similar results with other APC-dependent RNAs, such as *Pkp4* and *Kank2*.

In cells expressing FUS mutants that do not form inclusions (i.e., the protein is localized either in the nucleus or diffusely in the cytoplasm), the *Ddr2* RNA was peripherally distributed similarly to the control GFP-expressing cells (Fig. 1 B). Interestingly, though, in cells containing cytoplasmic FUS granules, the *Ddr2* RNA was mislocalized, indicated by a significant reduction in its edge ratio (Fig. 1 B). Formation of FUS granules similarly affected localization of another APC-dependent RNA (*Kank2*; Fig. S2 A) but did not reduce the edge ratio of a diffuse control RNA (*Arpc3*; Fig. S2 B). A similar effect was observed in the presence of inclusions formed by overexpression of the wild-type protein (Fig. S2 E), suggesting that it is mediated by inclusion formation and does not require the presence of specific mutations. Furthermore, the effect on RNA localization did not simply correlate with differences in the expression level of the mutant protein (Fig. S2 F). It was also not caused by

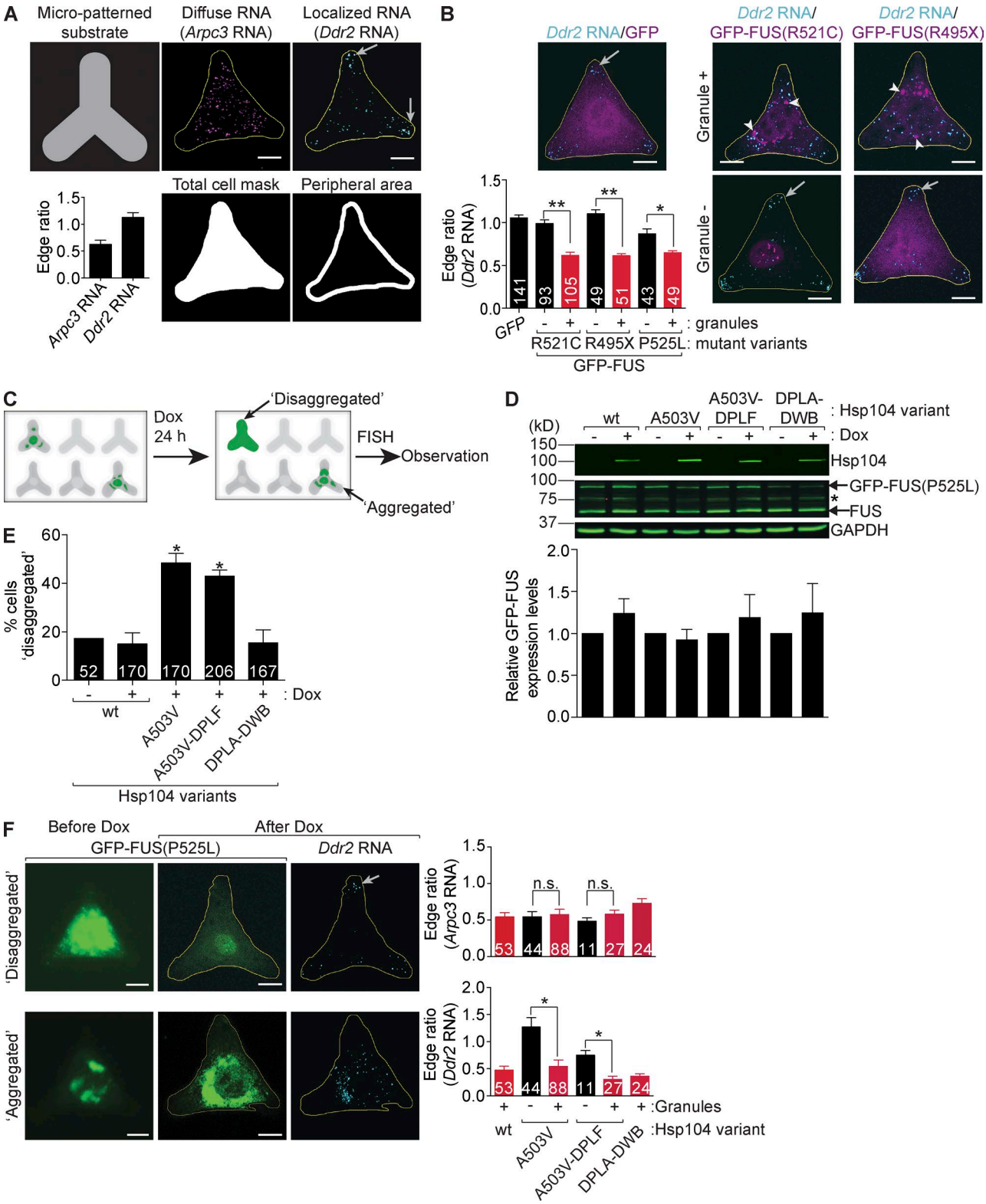

Figure 1. **ALS-associated FUS mutants mislocalize RNAs from cell protrusions in an inclusion-dependent manner.** (A) FISH of NIH/3T3 fibroblast cells to detect the indicated RNAs. The cells adopt a triangular shape on Y-shaped micropatterned substrates. The cell outline was used to derive the cell mask as well as a peripheral mask extending 2 µm from the outer cell perimeter. Edge ratios from a cell population were calculated as the fraction of RNA intensity in the peripheral mask normalized to the fraction of area in the peripheral mask. The APC-dependent localized RNA *Ddr2* exhibits a higher edge ratio than the nonlocalized control RNA *Arpc3*. (B) Representative images of *Ddr2* RNA FISH of cells expressing GFP, GFP-FUS(R521C), or GFP-FUS(R495X), without or with cytoplasmic granules (arrowheads), and edge ratio quantitations. Numbers within each bar indicate the total number of cells observed in independent experiments (five for GFP and GFP-FUS(R521C), one for GFP-FUS(R495X), and two for GFP-FUS(P525L)). (C) Schematic of experimental strategy for Hsp104-induced disaggregation. (D) WBs detecting the indicated proteins from induced or uninduced cells expressing Hsp104 variants. GFP-FUS levels, normalized to GAPDH, were expressed relative to doxycycline (Dox)-negative samples. There were no statistical differences between Dox^- and Dox^+

changes in the amount of total FUS protein in the nucleus because similar amounts of FUS were found in the nucleus in the presence or absence of inclusions (Fig. S2 G). Overall, these data indicate that cytoplasmic inclusions of FUS specifically affect the distribution of peripherally localized RNAs.

To directly test this idea and the role of FUS inclusions, we used engineered variants of the yeast Hsp104 protein disaggregase (Jackrel and Shorter, 2014; Jackrel et al., 2014). Potentiated Hsp104 variants (A503V and A503V-DPLF) can efficiently dissolve FUS aggregates in yeast and pure protein models, whereas the wild-type protein or a variant carrying mutations in the substrate-binding residues and the ATPase domain (DPLA-DWB) do not exhibit significant disaggregase activity (Jackrel and Shorter, 2014; Jackrel et al., 2014). We wanted to test whether dissolving FUS granules would restore RNA localization. For this, the different Hsp104 variants were placed under a doxycycline-inducible promoter and expressed together with GFP-FUS(P525L) (expression of this mutant results in a high proportion of inclusion-containing cells, thus facilitating the analysis). Cells with cytoplasmic FUS granules were marked on micropatterned substrates. Subsequently, expression of Hsp104 was induced for 24 h, and the same cells were scored for FUS disaggregation and *Ddr2* RNA localization (Fig. 1 C). All Hsp104 variants were expressed at similar levels and their expression did not significantly affect FUS expression (Fig. 1 D). Remarkably, expression of the two potentiated variants (A503V and A503V-DPLF) dissolved the cytoplasmic FUS granules in a large proportion of cells (Fig. 1 E). This finding establishes for the first time that potentiated Hsp104 variants can promote the dissolution of preformed inclusions of ALS-linked FUS in mammalian cells. Importantly, in these disaggregated cells, peripheral *Ddr2* RNA localization was restored (Fig. 1 F), confirming that the formation of cytoplasmic FUS inclusions disrupts RNA localization at cell protrusions. We note that because of resolution limits, we cannot exclude that some of the cells classified as "disaggregated" might still contain some undetectable inclusions. However, this would only lead to an underestimation of the rescuing effects we observed. We note also that ∼20% of the cells exhibit spontaneous disaggregation even in the absence of doxycycline and, supporting our conclusion, RNA localization is rescued in these cells (not depicted).

Cytoplasmic FUS inclusions disrupt the Glu-MT network

APC-dependent RNAs, localized at cell protrusions, are anchored at the plus ends of Glu-MTs (Mili et al., 2008). Therefore, to understand how formation of FUS inclusions leads to RNA mislocalization, we examined the Glu-MT network. Cells that did not exhibit visible FUS cytoplasmic granules showed no obvious effect on the overall MT cytoskeleton or the Glu-MT network (Fig. 2, A and B; and Fig. S2, C and D). In contrast, cells containing cytoplasmic FUS granules, induced by the expression of FUS mutants or overexpression of the wild-type FUS, showed a pronounced absence of Glu-MTs (Fig. 2, A and B; and Fig. S2, C and D). This effect was specifically directed toward Glu-MTs because no effect was observed on the levels of acetylated tubulin, another posttranslationally modified form of stable MTs (Fig. 2 C). Furthermore, the overall MT cytoskeleton and the distribution of dynamic MTs marked by EB1 appeared unperturbed (Fig. 2, B and C; and not depicted).

To test directly the role of FUS inclusions on MT stability, we again used the engineered Hsp104 variants. Indeed, dissolution of cytoplasmic FUS granules by the two potentiated Hsp104 variants (A503V and A503V-DPLF) increased the proportion of cells containing Glu-MTs (Fig. 2 D). Thus, we conclude that formation of cytoplasmic FUS granules disrupts the Glu-MT network and additionally leads to RNA mislocalization from protrusions.

Additional types of RNA-binding protein inclusions affect Glu-MTs and peripheral RNA localization

To test whether the Glu-MT network and peripheral RNAs are specifically affected by FUS inclusions, we induced formation of other types of RNA granules. Specifically, we examined cells exhibiting (a) inclusions formed upon overexpression of another ALS-related RNA-binding protein, TDP-43, carrying the patient-associated A315T mutation (Fig. 3, A and B), (b) stress granules induced by oxidative stress upon short exposure to sodium arsenite (Fig. 3, C and D), and (c) Dcp1 bodies formed through the exogenous expression of GFP-Dcp1α (Fig. 3 E). Cells containing TDP-43(A315T) inclusions showed a significant loss of the Glu-MT network and a reduction in peripheral RNA localization. These effects were not observed in cells without visible TDP-43 cytoplasmic inclusions (Fig. 3, A and B), similar to what was observed in the case of FUS. Comparable effects were also seen in the presence of stress granules (Fig. 3, C and D). However, importantly, no effect on the Glu-MT network was observed in the presence of Dcp1 bodies (Fig. 3 E). Therefore, loss of Glu-MTs and RNA mislocalization can be induced by some, but not all, types of RNA granules. It is interesting also that, as described in Figs. 8 and S4, FUS and TDP-43 granules likely bring about these similar phenotypic outcomes through distinct underlying mechanisms.

Glu-MTs are required for, and can promote, RNA localization at cell protrusions

Given the association of APC-dependent RNAs with Glu-MTs (Mili et al., 2008), it is likely that disruption of the Glu-MT network is responsible for the RNA localization defect upon formation of FUS inclusions. To test this, we modulated Glu-MT levels by manipulating the enzymes regulating their formation (Fig. 4 A). Glu-MTs are generated through the action of an unidentified TCP, which removes the C-terminal tyrosine of α-tubulin to expose a Glu residue (Hammond et al., 2008; Janke, 2014). TCP acts on polymerized MTs and, as a result, Glu-tubulin accumulates on stable MTs that are resistant to depolymerization (Glu-MTs; Kumar and Flavin,

groups by paired *t* test. *n* = 3–6. The asterisk indicates a nonspecific band. (E) Percentages of GFP-FUS(P525L)–disaggregated cells 24 h after induction of the indicated Hsp104 variants. Numbers within each bar indicate the total number of cells observed in four to five independent experiments apart from the Hsp104-uninduced wild-type (wt) sample, which was performed once. (F) Representative pre- and postinduction images of GFP-FUS(P525L) cells showing aggregation or disaggregation as well as *Ddr2* RNA FISH from same cells. Graphs are edge ratios of *Ddr2* or *Arpc3* RNAs. The total numbers of cells observed in two independent experiments are indicated within each bar. Similar results were obtained in two additional experiments in which Hsp104 expression was induced for shorter periods (12 or 18 h). (B, E, and F) *, $P < 0.002$; **, $P < 0.0001$; Mann–Whitney *U* test (B and F); and *, $P < 0.001$; compared with wt$^+$; Student's *t* test (E). Error bars show SEM. Bars, 10 µm. Arrows indicate RNA signals in protrusive areas.

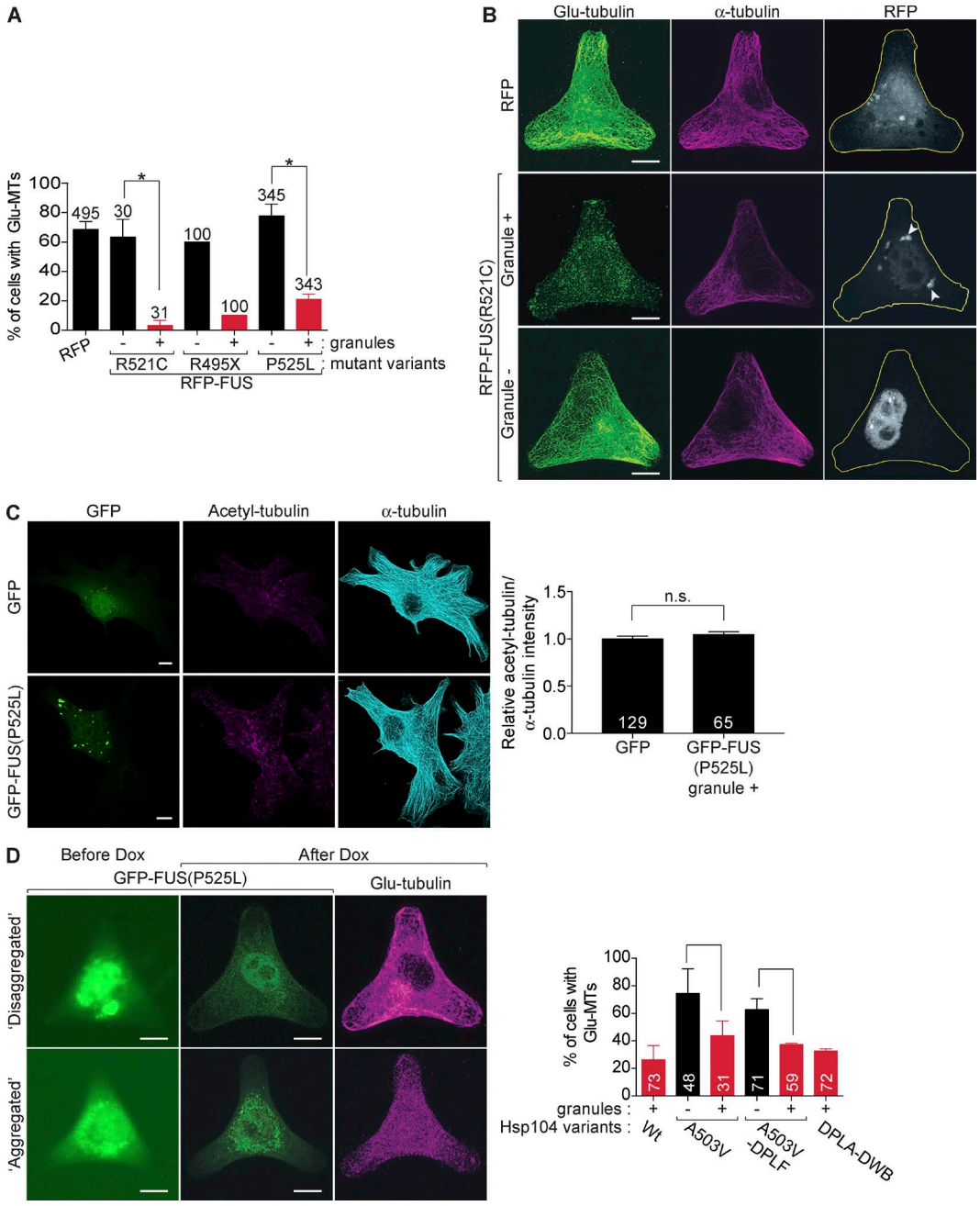

Figure 2. **Cytoplasmic FUS inclusions disrupt the detyrosinated MT network.** (A) Percentages of NIH/3T3 cells with Glu-MTs in the presence or absence of cytoplasmic FUS granules. Cells containing any visible Glu-MT fibers were considered Glu-MT–positive. The numbers above each bar indicate the total numbers of cells observed in independent experiments (three for RFP-FUS(R521C), one for RFP-FUS(495X), and four for RFP-FUS(P525L); each against a corresponding RFP control). *, $P < 0.0001$; Student's *t* test. (B) Representative IF images of total α-tubulin or Glu-tubulin in RFP and RFP-FUS(R521C) cells with or without cytoplasmic granules (arrowheads). (C) IF images of total α-tubulin and acetylated-tubulin in GFP and GFP-FUS(P525L) cells with cytoplasmic granules and quantification of relative intensities. The nonsignificant p-value was obtained by Mann–Whitney *U* test. (D) Representative images of Glu-tubulin staining in disaggregated and aggregated cells after Hsp104 induction, and quantitations of Glu-MT–positive cells from cells expressing the indicated Hsp104 variants. P-values between indicated pairs were $P = 0.0599$ (A503V) and $P = 0.0934$ (A503V-DPLF). (C and D) The total number of cells observed in two (C) or three (D) independent experiments is indicated within each bar. Error bars show SEM. Bars, 10 µm. Dox, doxycycline; Wt, wild type.

1981; Arce and Barra, 1985; Wehland and Weber, 1987). The chemical compound parthenolide inhibits TCP activity and prevents Glu-MT formation in cells (Fig. S3 A; Fonrose et al., 2007). Tubulin detyrosination can be reversed by tubulin-tyrosine ligase (TTL). TTL efficiently and exclusively retyrosinates soluble α/β-tubulin dimers such that newly assembled and dynamic MTs are predominantly tyrosinated (Tyr-MTs; Prota et al., 2013; Szyk et al., 2013; Janke, 2014). Therefore, reducing TTL function through TTL knockdown increases Glu-tubulin levels (Fig. S3 A).

Edge ratio quantitation was then used to assess how changes in Glu-tubulin levels affect APC-dependent RNA localization. Parthenolide treatment led to a significant decrease in the peripheral accumulation of *Ddr2* and *Kank2* RNAs but not of the control *Arpc3* RNA (Figs. 4 B and S3 B). In contrast, TTL knockdown increased peripheral *Ddr2* RNA amounts (Fig. 4 C).

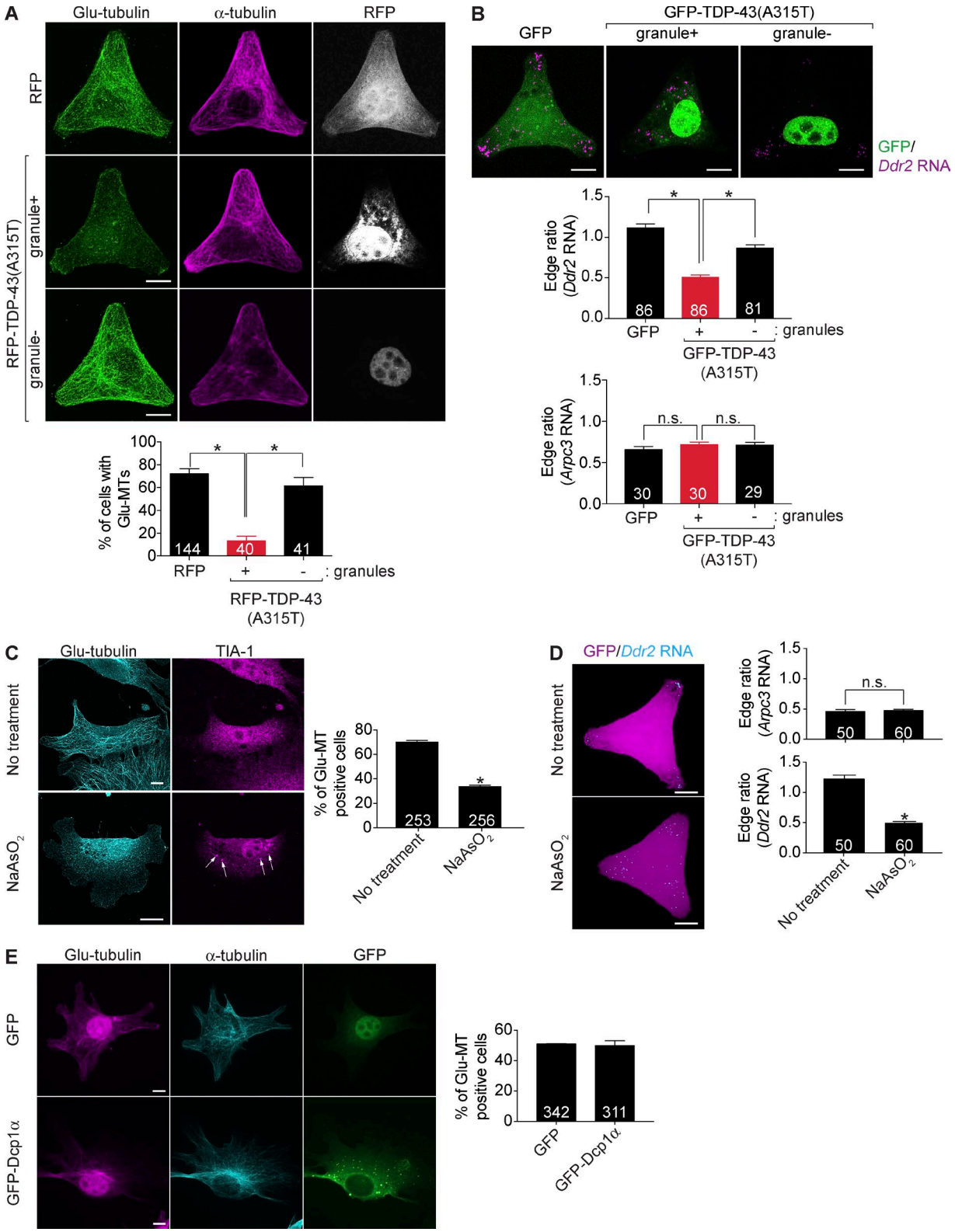

Figure 3. **TDP-43 inclusions and stress granules, but not Dcp1 bodies, disrupt Glu-MTs and RNA localization at protrusions.** (A) Representative IF images of total α-tubulin and Glu-tubulin of cells expressing RFP or RFP–TDP-43(A315T) and quantification of percentages of cells with Glu-MTs. (B) *Ddr2* or *Arpc3* RNA edge ratios of cells expressing GFP or GFP–TDP-43(A315T) with or without cytoplasmic granules. Numbers within each bar indicate the total number of cells observed in more than four independent experiments. (C and D) Cells treated or not treated with sodium arsenite were immunostained to detect Glu-tubulin and TIA-1–containing stress granules (arrows; C) or analyzed by FISH (D). (E) Representative IF images of total α-tubulin and Glu-tubulin of cells expressing GFP or GFP-Dcp1α and percentages of cells with Glu-MTs. (A and C–E) Numbers within each bar indicate the total number of cells observed in three independent experiments. (A–E) *, P = 0.0005; Student's *t* test (A); and *, P < 0.0001; Mann–Whitney *U* test (B and D) or Student's *t* test (C). There was no statistical difference by Student's *t* test in E. Error bars show SEM. Bars, 10 µm.

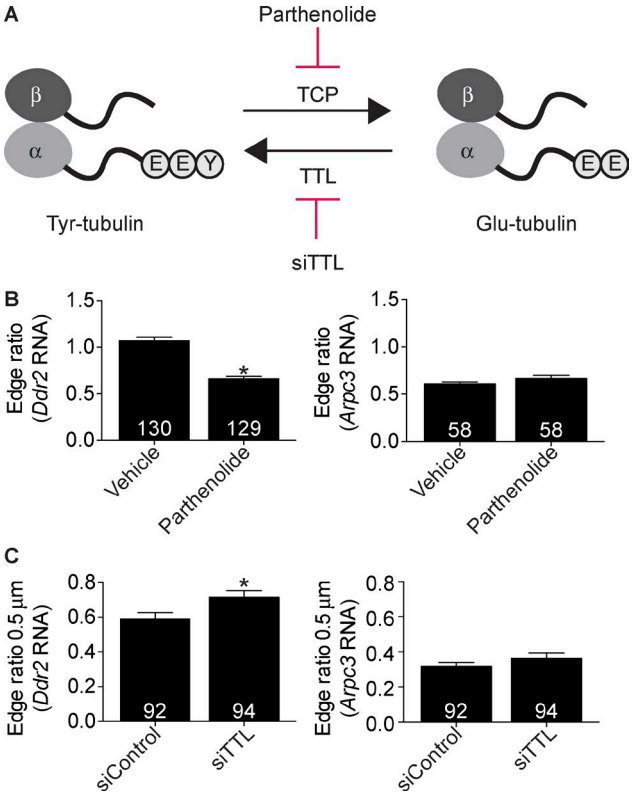

Figure 4. **Glu-MTs are required for and can promote RNA localization at cell protrusions.** (A) Schematic of the detyrosination cycle of α-tubulin. E, glutamate; Y, tyrosine. (B) Edge ratios of *Ddr2* RNA (left) *and Arpc3* RNA (right) from control and parthenolide-treated cells. (C) Edge ratios of *Ddr2* RNA (left) *and Arpc3* RNA (right) from control and TTL-knockdown cells. Note that, in this case, edge ratio is calculated using a 0.5-µm peripheral area to better allow the detection of enhanced RNA localization beyond the control baseline distribution, which is already quite peripheral. (B and C) *, $P < 0.0001$; Mann–Whitney *U* test. Numbers within each bar indicate the total number of cells observed in four independent trials for *Ddr2* RNA, two for *ArpC3* RNA (B), and two independent trials (C). Error bars show SEM.

These results indicate that Glu-MTs are required for and can, to a certain extent, promote RNA localization at cell protrusions. We note that the increase in *Ddr2* RNA edge ratio upon TTL knockdown does not appear proportional to the increase in Glu-tubulin (Fig. S3 A), potentially suggesting that an additional limiting factor or factors are required together with Glu-MTs to support RNA transport and/or anchoring to the periphery.

Kinesin-1 mRNA and protein are recruited in FUS granules

To identify additional factors involved in *Ddr2* RNA localization, we focused on the plus end MT motor kinesin-1 (KIF5) for the following reasons. The kinesin-1 family member, KIF5C, exhibits a preference for Glu-MTs (Dunn et al., 2008; Cai et al., 2009; Konishi and Setou, 2009), it is implicated in RNA transport events in neurons (Kanai et al., 2004), and it colocalizes with peripheral APC clusters (Dunn et al., 2008). In cells expressing mutant FUS, overall levels of KIF5B, which is the more abundant kinesin-1 isoform in fibroblast cells, do not change significantly (Fig. 5 A). However, IF staining of KIF5B or KIF5C using multiple antibodies revealed that both kinesin-1 isoforms were concentrated in cytoplasmic FUS granules (Fig. 5 B). Staining of siRNA-treated cells to knock down each isoform confirmed the specificity of the signals detected within inclusions (Fig. S3, C–E).

Given that FUS granules are thought to contain RNA and to affect RNA metabolism, we further investigated whether they also have an effect on the distribution of the kinesin-1 mRNA. Indeed, we find that cytoplasmic FUS granules are bona fide RNA granules, indicated by the accumulation of polyadenylated RNA visualized by in situ hybridization with oligo(dT) probes (Fig. 5 C). In situ hybridization to detect the *Kif5b* mRNA revealed that it was also enriched either within or in close proximity to FUS granules (Fig. 5 C). Interestingly, quantification of RNA levels found within FUS granules revealed that *Kif5b* mRNA preferentially partitioned within granules relative to the overall polyadenylated RNA population (Fig. 5 D). Furthermore, this was not accompanied by overall changes in *Kif5b* RNA levels (Fig. 5 E), indicating that partitioning of *Kif5b* mRNA within FUS granules is an active process and not a result of changes in RNA stability. Overall, these data indicate that formation of FUS granules leads to the recruitment of both *Kif5b* RNA and KIF5B protein within inclusions.

We cannot accurately assess the extent of KIF5B protein sequestration within inclusions because, to a large extent, the diffuse cytoplasmic signal detected through IF is nonspecific (Fig. S3 C). Nevertheless, it is interesting that various kinesins, including kinesin-1, are predicted to contain significant regions of intrinsically disordered regions (IDRs; Seeger and Rice, 2013). IDR interactions have been proposed to mediate the recruitment of proteins into phase-separated granules (Kato et al., 2012; Lin et al., 2015), suggesting the possibility that IDR interactions might mediate sequestration of kinesin in cytoplasmic FUS granules. Indeed, although we can observe accumulation of the full-length YFP-KIF5B into RFP-FUS(P525L) granules, deletion of the C-terminal IDR domain prevents accumulation of the truncated kinesin within FUS cytoplasmic inclusions (Fig. S3 F).

Kinesin-1 is required for the formation of Glu-MTs and RNA localization at cell protrusions

We hypothesized that sequestration of kinesin-1 into cytoplasmic FUS granules could disrupt its normal functions. To assess the functional contribution of kinesin-1, we knocked down KIF5B expression using two different siRNAs (Fig. S3 G). Knockdown of KIF5B, but not of the kinesin KIF3A, resulted in a significant reduction in the proportion of cells exhibiting a well-defined Glu-MT network (Fig. 6, A and B). We observed a similar reduction in Glu-MTs when expressing a dominant-negative kinesin-1 construct (KIF5B(ΔMD)), which lacks the N-terminal motor domain (Rivera et al., 2007). Therefore, KIF5B plays a necessary role in the formation of Glu-MTs. Furthermore, consistent with the requirement of Glu-MTs for *Ddr2* RNA localization described in Fig. 4 B, both KIF5B knockdown and dominant-negative expression reduced the peripheral localization of *Ddr2* RNA to levels similar to those exhibited upon FUS inclusion formation (Fig. 6, C and D).

FUS inclusions disrupt Glu-MTs and axonal RNA localization in primary neuronal cells

To determine whether FUS inclusions affect RNA localization through similar mechanisms in other cell types, we used primary hippocampal neurons. Mutant GFP-FUS expression was induced at day in vitro (DIV) 3, and cells were analyzed at DIV6.

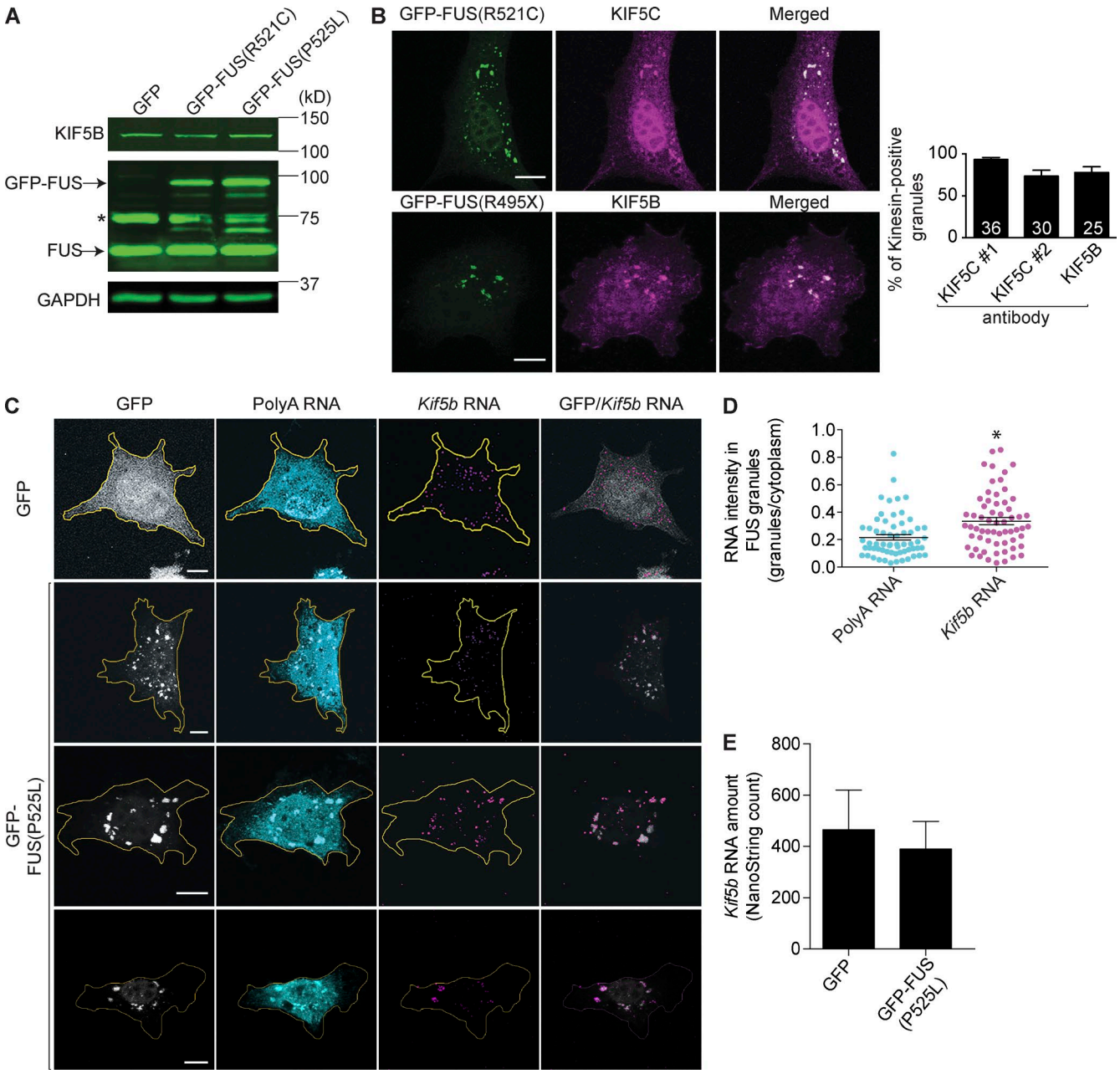

Figure 5. **Kinesin-1 RNA and protein are recruited in FUS granules.** (A) WBs of KIF5B expression in NIH/3T3 cells expressing GFP or GFP-FUS mutants. The asterisk indicates a nonspecific band. (B) Immunostaining of KIF5B or KIF5C in NIH/3T3 cells exhibiting mutant FUS cytoplasmic granules and corresponding quantitations. The number of cells observed from more than two independent trials is indicated within each bar. (C) *Kif5b* or polyA RNA FISH in cells with FUS granules. Yellow lines indicate cell outlines. (D) Signal intensity of *Kif5b* or polyA RNA within FUS granules normalized to total RNA signal intensity in the cytoplasm. (E) GFP- or GFP-FUS(P525L)–expressing cells were sorted based on GFP to increase the proportion of transfected cells. The *Kif5b* RNA amount was detected using the NanoString nCounter platform and normalized against the *Ldha*, *Rsp12*, and *Rpl35* RNA amounts. (D and E) *, $P < 0.0001$ (D); and no statistical difference (E); Student's *t* test. $n = 3$. Error bars show SEM. Bars, 10 µm.

As observed in fibroblasts, mutant GFP-FUS was detected in neuronal somas either diffusely in the cytoplasm or in inclusions (Fig. 7 A). At this stage, kinesin-1 was detected within somas and throughout the axonal compartment and growth cones. Expression of GFP-FUS(R495X) did not change total Kif5C expression levels (the predominant neuronal kinesin-1 isoform; Fig. 7 B) but led to a decrease in Kif5C levels at axon terminals, detected using two different antibodies (Fig. 7 C). Furthermore, IF staining showed a decrease in Glu-tubulin levels in axon terminals, similar to that observed after parthenolide treatment (Fig. 7 D). Interestingly, both of these effects are inclusion dependent, as they were not observed in cells exhibiting diffuse cytoplasmic GFP-FUS(R495X). To test for effects on RNA localization, we focused on the APC-dependent RNA *Dynll2* because it is more abundant in neurons. In control cells, the *Dynll2* RNA was distributed in somas and throughout axons. In the presence of mutant FUS inclusions, *Dynll2* axonal localization was significantly reduced (Fig. 7 E). Again, this was an effect induced by inclusions because *Dynll2* RNA presence in axons was not affected when mutant FUS(R495X) was

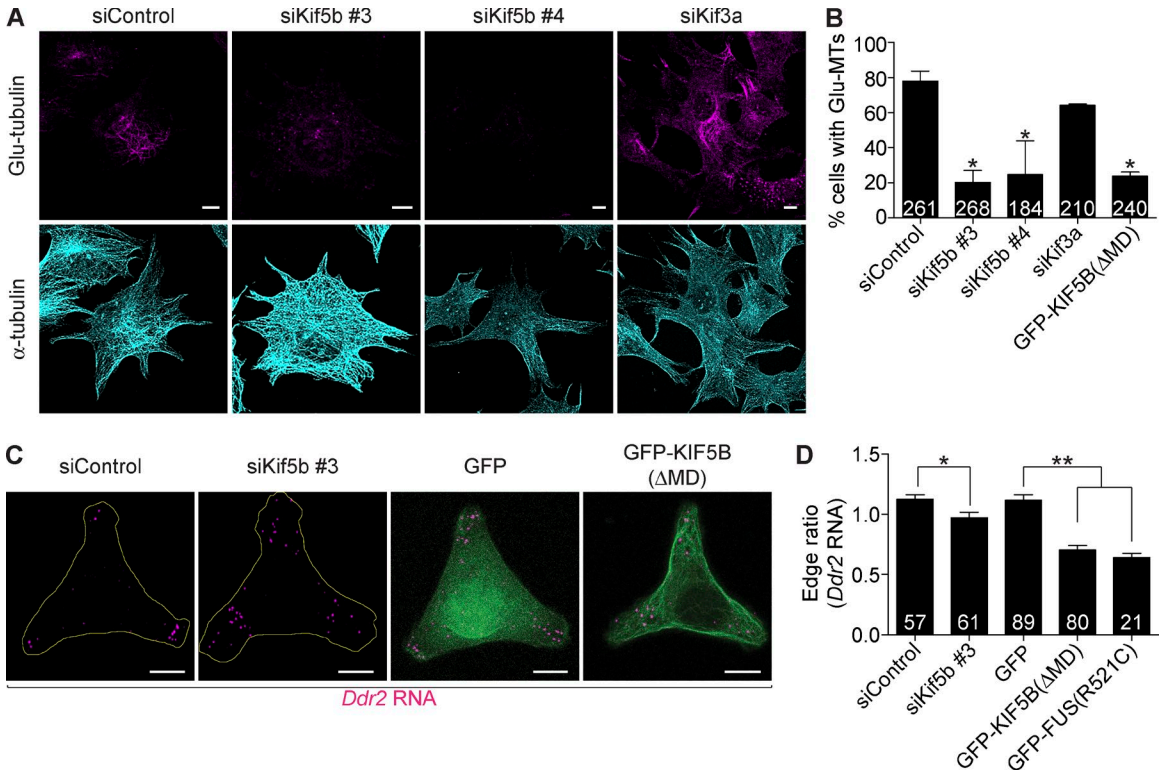

Figure 6. **Kinesin-1 is required for the formation of Glu-MTs and RNA localization at cell protrusions.** (A) Representative images of Glu-tubulin and α-tubulin staining of cells transfected with the indicated siRNAs. (B) Percentage of cells with Glu-MTs upon transfection with the indicated siRNAs or with a dominant-negative kinesin-1 construct. (C) Representative images of *Ddr2* RNA FISH of cells transfected with the indicated siRNAs or expressing GFP or GFP-KIF5B(ΔMD). (D) *Ddr2* RNA edge ratio of cells expressing the indicated siRNAs or GFP-tagged constructs. (B and D) Numbers of cells observed in two or more independent trials is indicated within each bar. *, $P < 0.05$; Student's *t* test compared with siControl (B); and *, $P = 0.0082$; **, $P < 0.0001$; Mann–Whitney *U* test or one-way analysis of variance using Dunnett's multiple comparisons test, respectively (D). Error bars show SEM. Bars, 10 µm.

diffusely distributed in the cytoplasm. We therefore conclude that, similar to fibroblasts, in neurons, cytoplasmic inclusions of FUS also trigger the same cascade of events, including misdistribution of kinesin-1 and loss of Glu-MTs, leading to the mislocalization of RNAs from the axonal compartment.

Overexpression of kinesin-1 is sufficient to rescue Glu-MTs and RNA localization in the presence of FUS, but not TDP-43, granules

Collectively, the aforementioned data indicate that, in different cell types, recruitment of kinesin-1 in cytoplasmic FUS granules is responsible for the observed loss of Glu-MTs and the subsequent mislocalization of RNAs from protrusive regions. To test this idea, we asked whether kinesin-1 overexpression could rescue Glu-MT formation and *Ddr2* RNA localization in cells exhibiting cytoplasmic FUS granules. For this, we overexpressed YFP-tagged KIF5B together with RFP-FUS(P525L) (Fig. 8 A). Consistent with the data shown in Fig. 5 (B–D), we observed that YFP-KIF5B can be detected within cytoplasmic FUS granules (Fig. S4 A). We note that this was only observed in some cells. We consider it likely that, depending on the level of overexpression, the increased amount of cytoplasmic YFP-KIF5B masks any YFP-KIF5B protein within FUS granules. As described in Figs. 1 B and 2 (A and B), in control cells, the presence of RFP-FUS(P525L) granules was accompanied by a significant reduction in the amount of cells with a visible Glu-MT network (Fig. 8, B and C) as well as a reduction in the peripheral accumulation of *Ddr2* RNA (Fig. 8, D and E). Importantly, however, overexpression of YFP-KIF5B led to significant rescue of both Glu-MTs and of peripheral RNA localization (Fig. 8, B–E). We additionally overexpressed untagged kinesin-1 and identified kinesin-1–overexpressing cells through detecting the amount of *Kif5b* RNA by in situ hybridization (Fig. S4 B). We observed a similar rescue of *Ddr2* RNA localization in the presence of FUS granules. These results strongly indicate that kinesin-1 recruitment within FUS granules is, to a large extent, responsible for the observed loss of Glu-MTs and RNA mislocalization phenotypes.

As shown in Fig. 3 (A and B), inclusions formed upon TDP-43(A315T) expression also disrupt Glu-MTs and *Ddr2* RNA localization. However, IF analysis showed that kinesin-1 was not appreciably recruited within TDP-43 inclusions (Fig. S4 C). Furthermore, overexpression of YFP-KIF5B did not rescue the loss of Glu-MTs or *Ddr2* RNA mislocalization in the presence of TDP-43 inclusions (Fig. S4, D and E). We cannot exclude that TDP-43 inclusions might affect kinesin-1 function in some other way, but these data suggest that kinesin-1 is not sufficient to restore their effects. Therefore, whereas FUS and TDP-43 inclusions lead to the same eventual outcomes, they likely do so through distinct underlying mechanisms.

Kinesin-1 promotes Glu-MT formation through directing TCP activity

We further sought to understand in more detail how FUS inclusions and kinesin-1 recruitment impact on the formation of Glu-MTs and whether independently modulating Glu-MT levels might be sufficient to overcome kinesin-1 sequestration. As

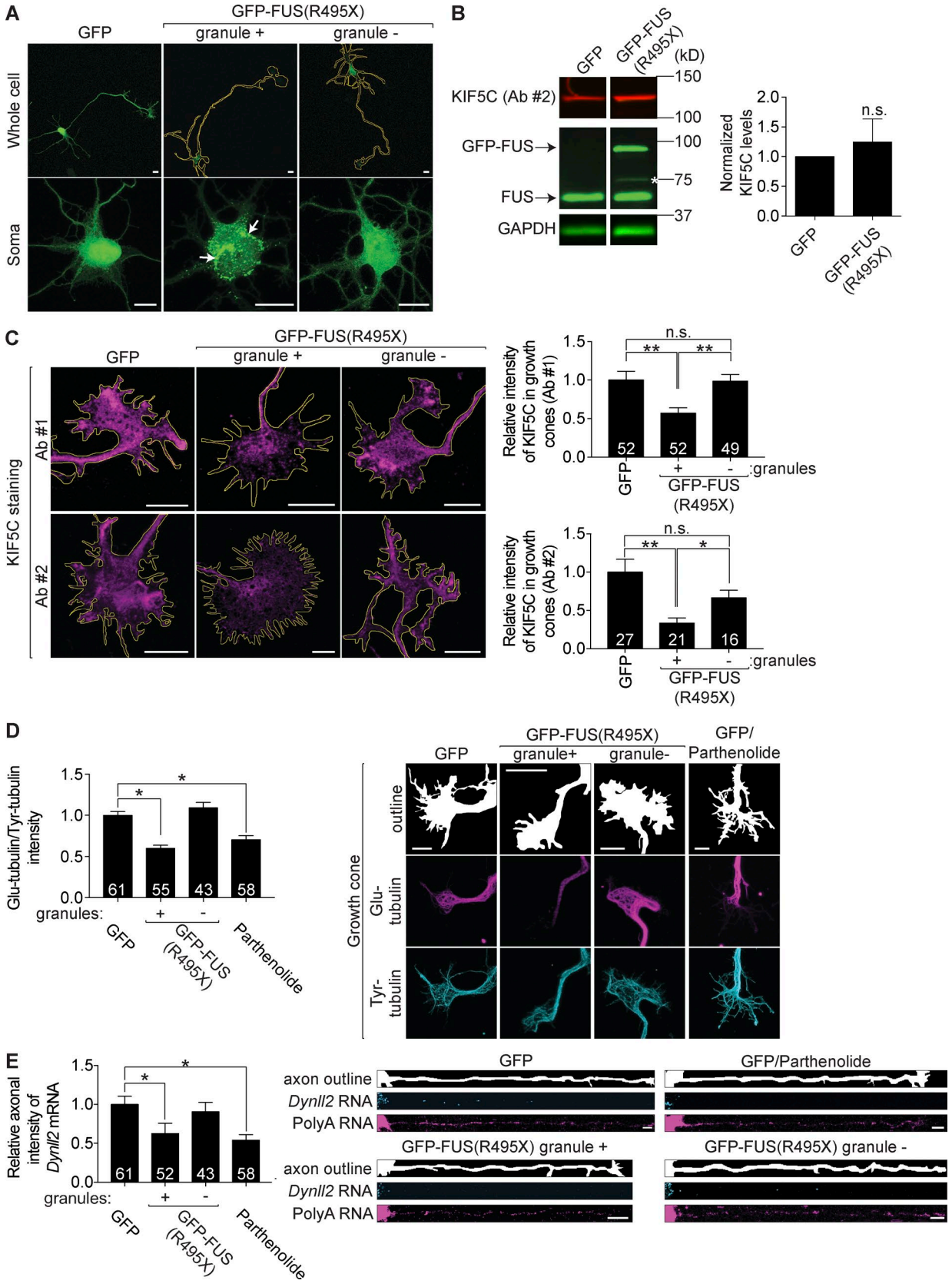

Figure 7. **FUS mutants disrupt KIF5C distribution, Glu-MTs, and axonal RNA localization in primary neuronal cells.** (A) Representative whole-cell images and enlarged soma views of DIV6 primary hippocampal neurons expressing GFP or GFP-FUS(R495X). Arrows indicate cytoplasmic FUS inclusions in soma; yellow lines indicate cell outlines. (B) Representative WBs and quantification of KIF5C levels in cells expressing GFP or GFP-FUS(R495X). The asterisk indicates a nonspecific band. (C) KIF5C immunostaining of DIV6 primary hippocampal neurons expressing GFP or GFP-FUS(R495X). KIF5C intensity in growth cones (yellow outlines) was normalized to growth cone area and expressed relative to the GFP sample. (D) DIV6 primary hippocampal neurons expressing

mentioned in Fig. 4 A, the levels of Glu-MTs result from the balance of the enzymatic activities involved in the tubulin detyrosination cycle. Knockdown of TTL shifts that balance and increases Glu-tubulin levels. We therefore tested whether TTL knockdown could offer an alternative way of restoring Glu-MT levels in cells with FUS inclusions and thus rescue *Ddr2* RNA localization. Interestingly, we found that in the presence of FUS inclusions, TTL knockdown was not sufficient to rescue *Ddr2* RNA localization at protrusions (Fig. 9 A).

To obtain a quantitative assessment of the effect of TTL knockdown on Glu-MTs, we measured Glu-tubulin levels by WB normalized in each case to total tubulin. We set the increase in Glu-tubulin levels upon TTL knockdown in control cells as 1.0 and compared the corresponding increase in Glu-tubulin upon different treatments (Fig. 9 B). In all cases, the extent of TTL knockdown was similar (Fig. S5 A). Interestingly, though, we found that in cells transfected with GFP-FUS(P525L), TTL knockdown led to a much smaller increase in Glu-tubulin levels (Fig. 9 B), considering also that ∼50% of the cells are expressing the transfected mutant FUS. This result is consistent with, and likely underlies, the lack of rescue in RNA localization upon TTL knockdown.

When TTL is knocked down, the level of increase of Glu-tubulin reflects the rate of Glu-tubulin generation or, in other words, the activity of the TCP (Fig. 4 A). Therefore, the reduced accumulation of Glu-tubulin upon TTL knockdown suggests that mutant FUS impacts tubulin modification likely by preventing the function of TCP. Additionally, similar to the effect of mutant FUS, KIF5B knockdown (but not KIF3A knockdown) also dampens the increase in Glu-tubulin induced upon TTL knockdown (Figs. 9 B and S5 A). This suggests that FUS inclusions and loss of kinesin-1 function are part of the same mechanism, which perturbs Glu-MT formation through affecting the action of TCP but not the activity of TTL.

A decrease in TCP action could be achieved by directly affecting TCP levels or activity or by preventing MT stabilization because TCP preferentially acts on stabilized MTs (Kumar and Flavin, 1981; Arce and Barra, 1985; Wehland and Weber, 1987). To distinguish between these possibilities, we first assessed MT stability by evaluating the decay of α-tubulin staining upon exposure to the MT-depolymerizing drug, nocodazole. As shown in Fig. 9 C, α-tubulin levels decayed with similar rates in control or FUS inclusion–containing cells, indicating that the presence of FUS inclusions does not overtly affect the levels of stable MTs. As an alternative way of assessing the role of MT stability, we tested whether in the presence of FUS inclusions, Glu-MT formation could be rescued by the stabilization of MTs upon taxol treatment. As expected, in control GFP-expressing cells, taxol treatment led to a significant increase in the total amount of detectable Glu-MTs. However, in the presence of GFP-FUS(P525L) granules, taxol treatment was not able to increase Glu-MT levels to the same extent (Fig. 9 D). In both cases, taxol had an equally stabilizing effect because acetylated tubulin levels exhibited a similar increase in the absence or presence of FUS inclusions (Fig. S5 B). Therefore, FUS inclusions and kinesin-1 sequestration appeared to mainly impact Glu-MT formation through a mechanism that does not involve MT stabilization but rather the function of TCP.

Given that the molecular entity of TCP is unknown, understanding this effect in more detail is difficult. However, a serendipitous observation provided a clue about a potential mechanism through which kinesin-1 affects TCP activity. A dominant-negative kinesin-1 construct, GFP-KIF5C(T93N), carries a point mutation that inhibits ATP hydrolysis and consequently binds but cannot move along MTs (Dunn et al., 2008). In agreement with a prior study (Dunn et al., 2008), we saw that GFP-KIF5C(T93N) decorated MTs at the perinuclear region and did not extend significantly to the periphery (Fig. 10 A). Interestingly, this kinesin mutant had a different effect on Glu-MTs. Although the GFP-KIF5B(ΔMD) dominant-negative kinesin mutant prevented Glu-MT formation (Fig. 6 B), the GFP-KIF5C(T93N) did not reduce Glu-MT levels but caused their perinuclear redistribution (Fig. 10, A and B). Importantly, GFP-KIF5C(T93N)–decorated MTs coincided with Glu-MTs (Fig. 10 A), indicating that KIF5 acts to either directly recruit or provide a signal for guiding TCP activity toward specific MTs.

To further test whether TCP targeting, rather than activity, is affected by the formation of FUS inclusions, we examined the effect of kinesin mutants in cells containing cytoplasmic FUS granules. Interestingly, even in the presence of FUS granules, expression of GFP-KIF5C(T93N) can rescue and direct the detyrosination of MTs on which it resides (Fig. 10 C), indicated by the appearance of Glu-tubulin staining which colocalized with GFP-KIF5C(T93N)–decorated MTs. The motor domain is required for this activity because GFP-KIF5B(ΔMD) did not rescue Glu-MTs (Fig. 10 C). These results suggest that FUS inclusions likely do not compromise the intrinsic activity of TCP, but rather prevent TCP targeting by recruiting kinesin-1 and inhibiting its ability to direct TCP activity on specific MTs. This in turn perturbs the transport and/or anchoring of APC-dependent RNAs, which rely on the Glu-MT network (Fig. 10 D).

Discussion

We describe in this study that APC-dependent RNA localization at cell protrusions was disrupted upon the formation of cytoplasmic FUS inclusions. This effect was observed in both fibroblasts and neuronal cells, and our data indicate that it is caused by the disruption of the MT motor kinesin-1 through the recruitment of both the kinesin-1 mRNA as well as of the kinesin-1 protein within FUS inclusions. Further delineating the underlying mechanism has led to the identification of a novel role of kinesin-1 in regulating the generation of Glu-MTs through targeting TCP activity. FUS inclusions thus lead to a loss of Glu-MTs and a subsequent mislocalization of APC-dependent RNAs, which require Glu-MTs for their localization (Fig. 10 D). The loss of Glu-MTs and RNA mislocalization were also observed in the presence of other types of inclusions (stress granules and TDP-43 inclusions); however, specificity

GFP or GFP-FUS(R495X) or treated with parthenolide were immunostained for Glu-tubulin and Tyr-tubulin. Glu-tubulin intensity in growth cones was normalized to Tyr-tubulin intensity and expressed relative to GFP samples. (E) FISH of *Dynll2* RNA and polyA RNA on DIV6 primary hippocampal neurons expressing GFP or GFP-FUS(R495X) or treated with parthenolide. Axonal intensity of *Dynll2* RNA was normalized to the axonal area and expressed relative to GFP samples. (C–E) *, $P < 0.0026$; **, $P < 0.0001$ (C); and *, $P < 0.0001$ (D and E); Mann–Whitney *U* test. (C and E) Numbers of cells observed in one (antibody #1), three (antibody #2; C), or two (E) independent trials are indicated within each bar. Error bars show SEM. Bars, 10 µm. Ab, antibody.

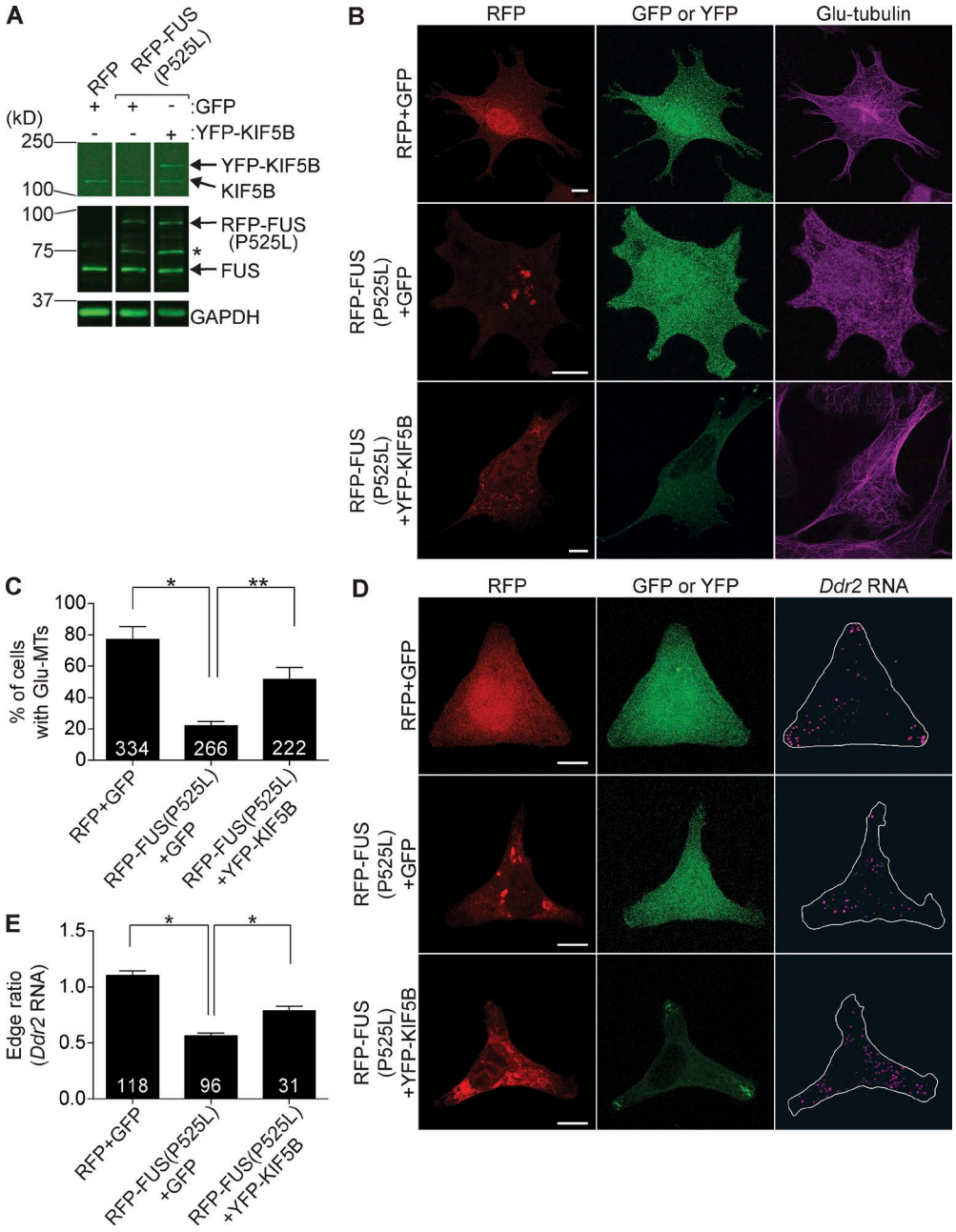

Figure 8. **Overexpression of KIF5B rescues Glu-MTs and RNA localization in the presence of FUS granules.** (A) NIH/3T3 cells transfected with RFP and GFP (first lane), RFP-FUS(P525L) and GFP (second lane), or RFP-FUS(P525L) and YFP-KIF5B (third lane) were analyzed by WB to detect the indicated proteins. The asterisk indicates a nonspecific band. (B) Representative images of cells transfected as in A and immunostained to detect Glu-tubulin. For RFP-FUS(P525L)–expressing cells, only cells exhibiting cytoplasmic FUS granules were imaged. (C) Percentages of cells with Glu-MTs from B were calculated. (D) Representative images of cells transfected as in A and analyzed by FISH to detect the *Ddr2* RNA. Cells exhibiting cytoplasmic RFP-FUS(P525L) granules were imaged. White lines indicate cell outlines. (E) Edge ratio values of cells from D. (C and E) Total numbers of cells observed in three independent trials is indicated within each bar. *, P = 0.003; **, P < 0.05; Student's *t* test (C); and *, P < 0.0001; Mann–Whitney *U* test. Error bars show SEM. Bars, 10 µm.

can be observed because Dcp1 bodies do not produce the same effects. Interestingly, TDP-43 inclusions did not recruit kinesin-1, and their effects were not suppressed by kinesin-1 overexpression, indicating that distinct types of inclusions lead to common outcomes through distinct mechanisms.

FUS belongs to an increasingly expanding group of proteins that contain disordered LCDs (King et al., 2012). These domains mediate a liquid–liquid phase separation that leads to the formation of membraneless compartments, which are reversible and dynamically controlled (Weber and Brangwynne, 2012; Courchaine et al., 2016; Protter and Parker, 2016). The dynamic properties of the granules in this study indicate that they have a significant dynamic component (Fig. S1 A). However, we cannot exclude that there was an immobile stable fraction akin to the stable core substructure reported for yeast and mammalian stress granules (Jain et al., 2016). Indeed, pathogenic ALS mutations in FUS or other RNA-binding proteins promote the conversion of dynamic liquid phases into stable, fibrillar, hydrogel structures that can retain other intrinsically disordered proteins (Kato et al., 2012; Lin et al., 2015; Molliex et al., 2015; Patel et al., 2015).

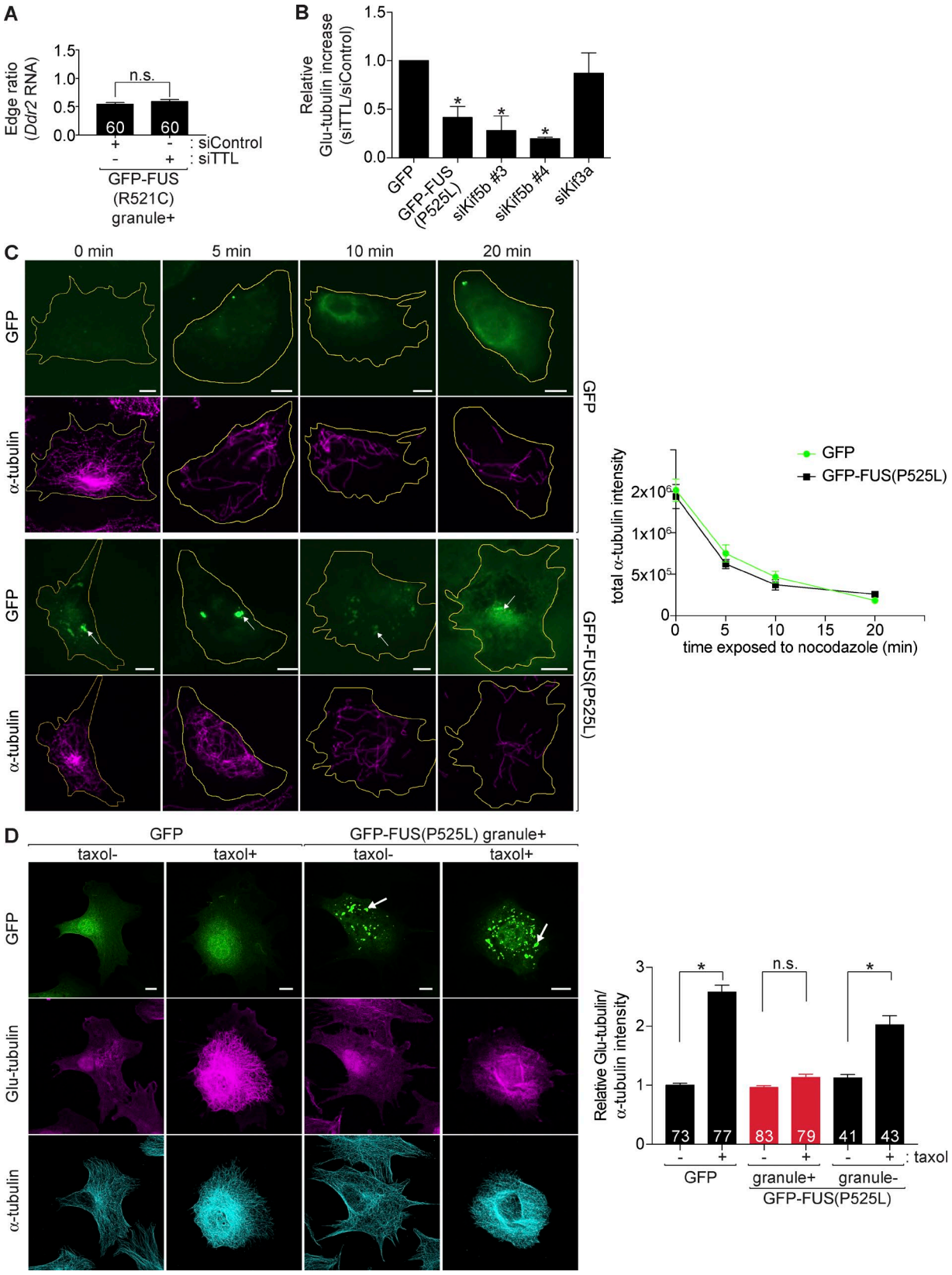

Figure 9. **FUS inclusions do not affect TTL activity or MT stabilization but rather impact the function of TCP.** (A) Edge ratio of *Ddr2* RNA from cells expressing GFP-FUS(R521C) and additionally transfected with control siRNAs or siRNAs against TTL. Only cells exhibiting cytoplasmic GFP-FUS(R521C) granules were analyzed. (B) Glu-tubulin levels were detected by WB and normalized to α-tubulin levels. The graph shows the increase in Glu-tubulin levels upon TTL knockdown (siTTL/siControl) from cells additionally expressing the indicated constructs or siRNAs. Results were expressed relative to the control sample of each trial. (C) Cells expressing GFP or GFP-FUS(P525L) were stained for α-tubulin after being exposed to nocodazole for the indicated minutes. Graph shows total tubulin intensity measured in >35 cells for each time point. Similar results were observed in two independent trials. Yellow lines indicate cell

FUS inclusions exhibit many common characteristics with stress granules, demonstrating retention of common proteins (e.g., TIA-1 and FMRP) as well as of polyadenylated mRNA. Nevertheless, as we show in this study, formation of FUS inclusions does not appear to be accompanied by the induction of a stress or unfolded protein response. This observation is consistent with studies showing that the neurotoxicity of FUS aggregates in *C. elegans* is not attributable to induction of unfolded protein response through PKR-like ER kinase (PERK) activation or to phosphorylation of eIF2α through other means (Murakami et al., 2015), as well as that phosphorylated PERK or IRE1 are not observed in FTLD-FUS cases, which exhibit FUS-positive inclusions (Nijholt et al., 2012).

Furthermore, whereas stress granules contain translationally stalled RNAs, FUS granules contain at least some translationally active mRNAs (Yasuda et al., 2013). Consistent with this, we observed that the recruitment of kinesin-1 mRNA within FUS inclusions did not lead to changes in kinesin-1 protein levels, indicating that the presence of kinesin-1 RNA within cytoplasmic inclusions is not accompanied by changes in its ability to be translated. The kinesin-1 protein is additionally concentrated within FUS inclusions, and our data suggest that its C-terminal intrinsically disordered region (Seeger and Rice, 2013) contributes to its retention. Kinesin-1 can additionally interact with APC (Ruane et al., 2016), which is also found within FUS inclusions. This interaction could provide an additional mechanism for retaining kinesin-1 within FUS granules or could act as a secondary way of perturbing APC-dependent RNA localization.

We show that kinesin-1 retention within FUS inclusions can be overcome upon its overexpression, leading to substantial rescue of Glu-MT formation and RNA localization. Although we cannot exclude that additional factors might be required, we believe that complete rescue was not observed because of the transient and thus variable expression range of both FUS and kinesin-1 in our system. An additional interesting observation is that KIF5B overexpression appears to affect the morphology of FUS inclusions (Fig. 8, B and D), causing them to appear less condensed. This might be related to the suggested role for kinesin-1 in the dissolution of stress granules (Loschi et al., 2009). It is possible that this effect is observed only when KIF5B reaches a certain expression threshold because endogenous KIF5B was found in condensed FUS granules (Fig. 5 B). We can only speculate about the nature of this effect. Assuming that FUS inclusions exhibit similar structural features to those of stress granules (Jain et al., 2016; Wheeler et al., 2016), it might be that KIF5B action affects the formation of a stable core or the interactions of the surrounding shell material with the core.

Members of the kinesin superfamily, in addition to their role in cargo transport, are known to also control MT dynamics, promoting either MT stabilization or destabilization (Jaulin and Kreitzer, 2010; Morris et al., 2014). The mechanism underlying kinesin-driven MT stabilization is not known, but an interaction with plus end tracking proteins has been implicated. We suggest here that kinesin-1 has a role in promoting MT detyrosination, but our data indicate that kinesin-1 does not promote detyrosination indirectly through promoting MT stabilization, but that it rather functions to recruit and/or target TCP on MTs. Testing this model more directly is challenging, given that the exact molecular entity of TCP has remained elusive, even though the biochemical activity of TCP has been identified several years ago (Janke, 2014).

The mechanism described here additionally provides new insights into molecular consequences that could be relevant for ALS pathology. Loss of Glu-MTs upon formation of FUS or TDP-43 inclusions results in the disruption of peripheral localization of APC-dependent RNAs. Indeed, APC supports the localization of RNAs in neuronal axons (Preitner et al., 2014), and reduced RNA transport and/or translation in axon terminals has been observed in response to ALS mutations in FUS and TDP-43 (Alami et al., 2014; Coyne et al., 2014, 2015; Murakami et al., 2015). Defects in axonal RNA translation could affect the transmission of survival signals to the cell soma and axonal regeneration and could also contribute to ALS pathogenesis (Liu-Yesucevitz et al., 2011; Jung et al., 2012; Yasuda and Mili, 2016).

Although the exact functional roles of APC-dependent RNAs are not known, the Rab13 protein, encoded by an APC-dependent RNA, is up-regulated in axonal sprouts and is important for nerve regeneration upon injury (Di Giovanni et al., 2006). Furthermore, RNA targets of APC, identified from mouse brain tissue by high-throughput sequencing of RNA isolated by cross-linking immunoprecipitation, include RNAs encoding tubulin isotypes and MT regulators, and their mislocalization affects MT dynamics (Preitner et al., 2014). This might suggest the interesting possibility that an initial disruption of Glu-MTs could be amplified or reinforced through disrupting the local translation of MT regulators. Similar feedback effects could occur in the case of other ALS mutations in the *TDP-43* gene. In *Drosophila melanogaster* motor neurons, TDP-43 mutations affect the transport and translation of *futsch* RNA, which encodes a protein homologous to mammalian MAP1B and which regulates MT organization (Coyne et al., 2014; Yasuda and Mili, 2016).

Loss of Glu-MTs and their downstream effects could be widespread features of ALS initiated by other genetic causes. ALS-associated mutations in the *SOD1* gene as well as in the gene encoding the tubulin isoform TUBA4A have also been associated with the presence of hyperdynamic destabilized MTs (Fanara et al., 2007; Smith et al., 2014). Thus, changes in MT dynamics and their ensuing effects might be a broader common denominator in ALS pathogenesis. Reduced stability and changes in the dynamic properties of MTs have also been associated with additional neurodegenerative diseases, and supporting their pathogenic relevance, approaches to restore MT stability have exhibited therapeutic potential (Yoshiyama et al., 2003; Zhang et al., 2005; Barten et al., 2012; Brunden et al., 2014). Our data support the therapeutic prospect of Hsp104-based disaggregases and additionally offer the restoration or manipulation of kinesin-1 activity as an alternative approach to reestablishing functional levels of stable modified MTs and reversing pathogenic phenotypes.

outlines. (D) Immunostaining of Glu-tubulin and α-tubulin in GFP- or GFP-FUS(P525L)–expressing cells treated or not treated with taxol. Glu-tubulin intensity was normalized to α-tubulin and expressed relative to the GFP sample. (C and D) Arrows indicate cytoplasmic FUS inclusions. (A, B, and D) Numbers in bars indicate the amounts of cells observed in two (A and D) or two to five (B) independent experiments. (A–D) *, $P < 0.0001$; Mann–Whitney *U* test (A and D); *, $P < 0.04$; paired Student's *t* test compared with GFP (B); and no statistical difference between GFP and GFP-FUS(P525L) by two-way analysis of variance using Bonferroni's multiple comparisons test (C). Error bars show SEM. Bars, 10 µm.

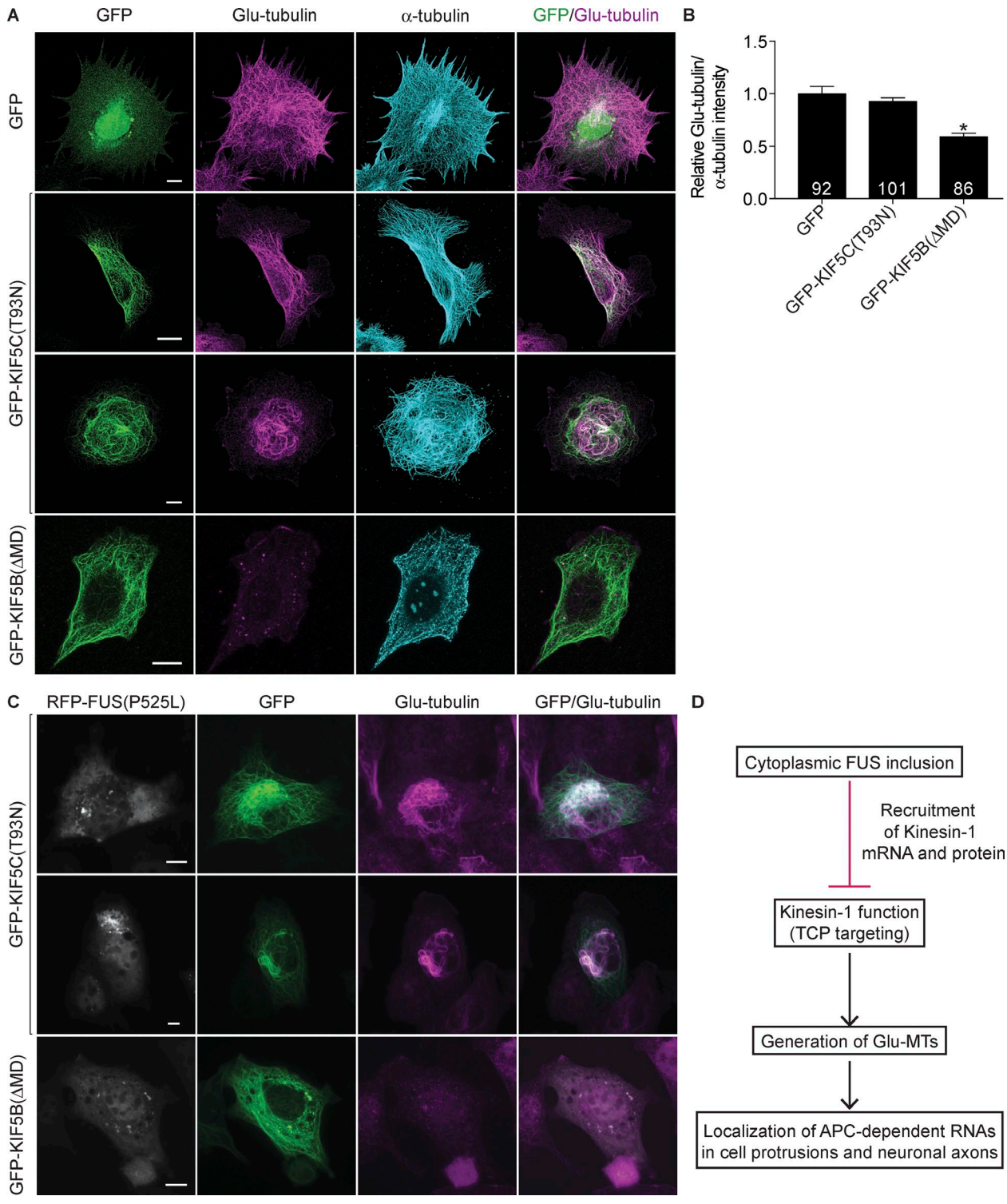

Figure 10. **Kinesin-1 promotes Glu-MT formation through directing TCP activity.** (A) Immunostaining of Glu-tubulin and α-tubulin in GFP-, GFP-KIF5C(T93N)–, or GFP-KIF5B(ΔMD)–expressing cells. (B) Glu-tubulin intensity of cells from A was normalized to α-tubulin intensity and expressed relative to the GFP sample. Numbers of cells observed in more than three independent trials are indicated. *, $P < 0.0001$; Mann–Whitney *U* test compared with GFP. Error bars show SEM. (C) Immunostaining of Glu-tubulin in GFP-KIF5C(T93N)– or GFP-KIF5B(ΔMD)–expressing cells cotransfected with RFP-FUS(P525L). Cells exhibiting cytoplasmic RFP-FUS(P525L) granules were imaged. Bars, 10 µm. (D) Proposed model of effects initiated by formation of FUS inclusions. Formation of cytoplasmic FUS inclusions leads to the recruitment of kinesin-1 RNA and protein. Our results indicate that kinesin-1 promotes Glu-MT formation by targeting the TCP activity. Sequestration within FUS inclusions disrupts this function of kinesin-1, resulting in a loss of Glu-MTs, which are in turn required to support localization of APC-dependent RNAs at cell protrusions and neuronal axons.

Materials and methods

Plasmid constructs

For transient expression, the FUS coding sequence, with or without the indicated mutations and tagged with GFP or RFP, was cloned into the pEGFP-C1 vector backbone. Constructs were described previously (Yasuda et al., 2013). For lentiviral transduction, the coding sequences of codon-optimized constructs of Hsp104 variants (sequence provided in the next section) or GFP-FUS mutants were cloned into pENTR1A vector and then transferred into pINDUCER20 lentivector using the Gateway LR clonase II Enzyme mix (11791-020; Thermo Fisher Scientific) according to the manufacturer's instructions. GFP-TDP-43(A315T) was provided by B. Wolozin (Liu-Yesucevitz et al., 2010). The coding sequence was digested with BamHI and XbaI and ligated into pEGFP-C1 vector, in which the GFP sequence was replaced with that of mRFP to generate an RFP-tagged TDP-43 mutant. GFP-Dcp1α was provided by J. Lykke-Andersen (University of California, San Diego, La Jolla, CA). pKin1b plasmid (31604; Addgene) was used to express untagged KIF5B protein. KIF5B(ΔMD) lacking amino acids 2–366 was generated by PCR from the pKin1b plasmid, and the PCR product was cloned into EGFP-C1 vector. KIF5B(ΔIDR) lacking amino acids 822–963 was generated by PCR from YFP-KIF5B and cloned into EGFP-C1. GFP-KIF5B(T93N) was provided by M. Peckham (Dunn et al., 2008). YFP-KIF5B was provided by D.B. Arnold (Rivera et al., 2007).

Nucleotide sequence of codon-optimized HSP104 for expression in mammalian cells

5′-ATGAATGACCAGACCCAGTTTACAGAAAGAGCCCT
GACCATCCTGACCCTGGCACAGAAGCTGGCATCCGA
CCACCAGCACCCACAGCTGCAGCCCATCCACATTCTG
GCCGCTTTCATTGAAACTCCCGAGGACGGGAGCGTG
CCTTACCTGCAGAACCTGATCGAGAAGGGCAGGTAC
GACTACGACCTGTTTAAGAAAGTGGTCAACCGAAAT
CTGGTGAGGATTCCTCAGCAGCAGCCAGCACCTGCA
GAGATCACCCCAAGCTACGCCCTGGGCAAGGTGCTG
CAGGACGCAGCCAAAATCCAGAAGCAGCAGAAAGAC
AGCTTCATTGCACAGGATCATATCCTGTTCGCCCTGTT
TAATGATAGCTCCATCCAGCAGATTTTCAAGGAAGCC
CAGGTGGACATCGAGGCTATTAAGCAGCAGGCACTG
GAGCTGCGGGGGAACACCAGAATCGACTCCCGCGGC
GCTGATACCAATACACCCCTGGAGTACCTGTCTAAA
TATGCTATTGATATGACCGAACAGGCACGGCAGGGC
AAGCTGGACCCTGTCATCGGAAGAGAGGAAGAGATT
CGATCAACAATCAGGGTGCTGGCCAGGCGGATCAAA
AGCAACCCATGCCTGATTGGAGAGCCCGGGATCGGC
AAGACAGCTATCATTGAAGGGGTGGCACAGCGCATC
ATTGACGATGACGTGCCAACTATCCTGCAGGGCGCC
AAGCTGTTCAGCCTGGATCTGGCTGCACTGACCGCT
GGCGCAAAATACAAGGGAGACTTCGAAGAGAGGTTT
AAGGGAGTCCTGAAAGAGATTGAAGAGTCCAAGACT
CTGATCGTGCTGTTTATCGATGAGATTCACATGCTGA
TGGGAAACGGGAAAGATGACGCCGCTAATATCCTGA
AGCCTGCCCTGAGCCGGGGGCAGCTGAAGGTCATTG
GCGCTACCACAAACAATGAATACAGATCCATCGTCGA
GAAAGACGGCGCCTTCGAAAGACGCTTTCAGAAGATT
GAAGTGGCTGAGCCATCCGTGAGACAGACAGTCGCA
ATCCTGCGCGGCCTGCAGCCCAAGTATGAGATTCAC
CACGGCGTGAGAATCCTGGACTCTGCACTGGTCACT
GCAGCCCAGCTGGCCAAGAGATACCTGCCTTATCGA
AGGCTGCCAGACAGCGCCCTGGACCTGGTGGATATC
TCCTGTGCTGGAGTGGCAGTGGCCAGGGACAGTAAA
CCTGAAGAGCTGGACTCAAAGGAGCGACAGCTGCAG
CTGATTCAGGTGGAAATCAAGGCCCTGGAACGGGAT
GAGGACGCTGATAGTACTACCAAGGATAGGCTGAAA
CTGGCCCGGCAGAAAGAGGCTTCACTGCAGGAAGAG
CTGGAACCACTGAGGCAGCGGTACAACGAAGAGAAG
CACGGACATGAAGAGCTGACACAGGCCAAGAAAAAG
CTGGACGAGCTGGAAAACAAGGCCCTGGACGCAGAG
CGGAGATACGATACTGCAACCGCTGCAGACCTGAGA
TATTTCGCCATCCCAGATATCAAGAAGCAGATCGAA
AAGCTGGAGGACCAGGTGGCAGAAGAGGAACGACGA
GCAGGAGCCAACTCTATGATTCAGAATGTGGTGGAC
TCAGATACAATCAGCGAGACTGCCGCTCGGCTGACC
GGCATTCCCGTGAAAAAGCTGTCCGAGTCTGAAAAC
GAGAAGCTGATCCACATGGAGAGGGACCTGAGCAGC
GAAGTGGTCGGCCAGATGGACGCCATCAAAGCCGTG
AGCAACGCCGTCAGACTGAGTCGCTCAGGCCTGGCC
AATCCACGACAGCCAGCTAGTTTCCTGTTTCTGGGA
CTGAGCGGCTCCGGAAAGACAGAGCTGGCAAAAAAG
GTGGCCGGGTTCCTGTTTAACGACGAGGATATGATG
ATCAGAGTGGATTGCTCTGAACTGAGTGAGAAATAC
GCTGTCAGTAAGCTGCTGGGCACAACTGCAGGATAC
GTGGGGTATGACGAGGGCGGATTCCTGACTAATCAG
CTGCAGTACAAACCTTATAGCGTGCTGCTGTTTGAT
GAAGTCGAGAAGGCCCACCCAGACGTGCTGACCGTC
ATGCTGCAGATGCTGGATGACGGAAGGATTACCAGC
GGGCAGGGCAAGACAATCGACTGCTCTAACTGTATC
GTGATTATGACAAGTAACCTGGGAGCCGAGTTCATT
AATTCCCAGCAGGGGTCTAAAATCCAGGAATCTACT
AAGAACCTGGTCATGGGGGCTGTCCGGCAGCATTTC
AGACCCGAGTTTCTGAACCGCATCTCAAGCATCGTG
ATTTTCAATAAGCTGAGCAGGAAAGCCATCCACAAG
ATTGTGGACATCCGACTGAAGGAGATCGAGGAAAGG
TTCGAACAGAACGATAAGCATTATAAACTGAATCTG
ACCCAGGAGGCAAAAGACTTTCTGGCCAAGTACGGA
TATAGCGATGACATGGGGGCCCGCCCTCTGAACCGA
CTGATTCAGAACGAGATCCTGAACAAGCTGGCCCTG
CGCATTCTGAAGAACGAAATCAAAGATAAGGAGACC
GTGAATGTGGTCCTGAAAAAGGGAAAGTCCAGGGAC
GAGAACGTGCCCGAGGAAGCAGAGGAATGTCTGGAG
GTCCTGCCTAATCACGAAGCTACAATCGGGGCTGAC
ACTCTGGGAGACGACGATAACGAGGATAGTATGGAG
ATTGACGATGACCTGGACTAATAA-3′.

Cell culture and transfection

NIH/3T3 cells were cultured in DMEM containing 10% calf serum, sodium pyruvate, and penicillin/streptomycin. Plasmid constructs were transfected using Lipofectamine 2000 (11668027) or Lipofectamine 3000 (L3000008; Thermo Fisher Scientific) according to the manufacturer's instructions, and cells were analyzed 24–48 h after transfection.

siRNAs used were as follows: siKif5B #3 (target sequence 5′-CAGCAAGAAGTAGACCGGATA-3′; SI02687412), siKif5B #4 (target sequence 5′-CACGAGCTCACGGTTATG CAA-3′; SI02733437), siKif3a #2 (target sequence 5′-ACG AACCTCCAAAGACATTTA-3′; SI00175994), siTTL #3 (target sequence 5′-CACCGCAAGTTTGACATTCGA-3′; SI01458331), siKif5C #2 (target sequence 5′-CGAAGTCAG TTTCCAAGATAA-3′; S100176071), and AllStars negative control siRNA (1027281; QIAGEN). siRNAs, 40 pmol at final concentration, were transfected into NIH/3T3 cells with

Lipofectamine RNAiMAX (13778-150; Thermo Fisher Scientific) according to the manufacturer's instructions. Cells were incubated for 3 d and retransfected with the same siRNA to enhance the knockdown efficiency. Cells were analyzed 6 d after initial transfection.

For generation of stable cell lines expressing Hsp104 variants, NIH/3T3 cells were transduced with the corresponding pINDUCER20 lentivectors, and infected cells were selected with 0.5 mg/ml Geneticin (Thermo Fisher Scientific). Protein expression was induced by the addition of 1 µg/ml doxycycline (Thermo Fisher Scientific).

For isolation of primary hippocampal neurons, brains were surgically dissected from E18 rat embryos. Hippocampi were isolated in dissection buffer (HBSS containing 10 mM Hepes, pH 7.3, penicillin, and streptomycin) and trypsinized with dissection buffer containing 0.25% trypsin and 0.025% DNase I for 15 min at 37°C. Cell suspension was triturated, and single cells were isolated after passing through a cell strainer (352350; Falcon). Dissociated neurons were plated onto coverslips coated with 1 mg/ml poly-L-lysine and cultured in NB27 media (neurobasal media [21103-049] with B27 supplements [17504-044], 10% FBS, penicillin/streptomycin, and GlutaMAX [35050-061; Thermo Fisher Scientific]). Media were changed within 12 h after plating and every third day after that. Exogenous proteins were expressed through lentiviral transduction. For infection with pINDUCER20 lentivectors, cells were centrifuged with virus at an MOI of 20 at 800 *g* for 10 min. At DIV3, 5 µM AraC (251010-1G; EMD Millipore) was added to reduce the glial cell population and doxycycline was added to induce transgene expression.

Parthenolide (P0667-5MG; Sigma-Aldrich) was added to 5 µM for 2–4 h for NIH/3T3 cells and 10 µM for 8 h for hippocampal neurons. Taxol (580555-5MG; EMD Millipore) was added to 10 µM for 2–4 h. Sodium arsenite (35000-1L-R; Fluka Analytica) was added to 500 µM for 1 h. Thapsigargin (T9033; Sigma-Aldrich) was added to 5 µM for 3 h.

Virus production and titration

Lentivirus was produced in HEK293T cells cultured in DMEM containing 10% FBS and penicillin/streptomycin. Cells were transfected with pINDUCER20 lentivectors together with packaging plasmids pMD2.G and psPAX2 using the PolyJet In Vitro DNA Transfection Reagent (SignaGen) for 48 h. Harvested virus was precipitated with polyethylene glycol at 4°C overnight. The viral pellet was resuspended in cell culture media and stored at −70°C. Virus was tittered by counting Hsp104-positive staining units or GFP-positive units after infection of HEK293T cells.

RNA FISH

For FISH, NIH/3T3 cells were plated onto fibronectin-coated micropatterned substrates called CYTOOchips (C15-1964; CYTOO). Neurons were plated at 20,000 cells per 18-mm coverslip coated with poly-L-lysine. Cells were fixed with 4% PFA in PBS (4% sucrose was also added for neuron fixation) for 15 min at RT.

FISH was performed with the QuantiGene ViewRNA ISH Cell Assay kit (QVCM0001; Affymetrix) according to the manufacturer's instructions. The following Affymetrix probe sets were used: *Ddr2* (VB1-14375-01), *Kank2* (VB1-14376-01), *Arpc3* (VB1-14507-01), and *Kif5b* (VB1-19715). To detect PolyA RNAs, locked nucleic acid–modified oligo(dT) probes (30 nucleotides) labeled with ATTO 655 were added during the hybridization, preamplification, amplification, and last hybridization steps of the QuantiGene ViewRNA ISH Cell Assay. For edge ratio analysis, cells were stained with CellMask Blue Stain (H32720; Thermo Fisher Scientific) instead of DAPI. Samples were mounted on slide glass with ProLong Gold antifade reagent (P36930; Thermo Fisher Scientific).

RNA isolation and analysis

For *Kif5b* RNA detection, NIH/3T3 cells were transfected with EGFP-C3 or GFP-FUS(P525L) plasmids using Lipofectamine 2000. 1 d after transfection, GFP-expressing cells were isolated though fluorescence-activated cell sorting, and RNA was extracted with TRIzol LS reagent (10296010; Thermo Fisher Scientific) according to the manufacture's instructions. Isolated RNA was treated with RQ1 RNase-free DNase (M6101; Promega) and analyzed using a custom-made codeset for the nCounter system (NanoString Technologies). Data were processed using nSolver analysis software (NanoString Technologies).

For *Kif5c* RNA detection, NIH/3T3 cells were transfected with control siRNAs or siRNAs against *Kif5c* using Lipofectamine RNAiMAX. 3 d later, RNA was extracted with TRIzol reagent. Isolated RNA was treated with RQ1 RNase-free DNase. cDNA was synthesized using the iScript cDNA Synthesis kit (1708891; Bio-Rad Laboratories) according to the manufacturer's instructions. cDNAs were used for PCR with Power SYBR Green PCR master mix (4367659; Applied Biosystems), and amplification was detected by the 7900HT Fast Real Time PCR System (Thermo Fisher Scientific). The detected RNA amount was normalized to the *GAPDH* RNA amount via ΔΔCt calculation. cDNAs were also used to amplify the spliced and unspliced versions of XBP1 RNA using Taq DNA Polymerase 2× Master Mix Red (180301; Amplicon). PCR products were run on Tapestation with D1000 Screen Tape (5067-55582; Agilent Technologies). Primers used were as follows: Kif5c forward, 5′-AGATTTGCGCTGTGAAACTCC-3′, and reverse, 5′-GCA TTCTCCTTGGCCTCTTT-3′; mXBP1 forward, 5′-AAACAG AGTAGCAGCGCAGACTGC-3′, and reverse, 5′-TCCTTC TGGGTAGACCTCTGGGAG-3′; and GAPDH forward, 5′-CCACCCAGAAGACTGTGGAT-3′, and reverse, 5′-CACATT GGGGGTAGGAACAC-3′. For quantitative PCR quantitation of spliced XBP1 RNA, primers that specifically amplify the spliced form were used according to van Schadewijk et al. (2012); XBP1–quantitative PCR forward, 5′-TGCTGAGTC CGCAGCAGGTG-3′ [the underlined sequence has mismatch to unspliced XBP1 mRNA so that it specifically amplifies the spliced form]; and XBP1–quantitative PCR reverse, 5′-GCTGGCAGGCTCTGGGGAAG-3′).

WB and IF

Antibodies used were as follows: rabbit anti-GAPDH (1:1,000 dilution for WB; 2118; Cell Signaling Technology), rabbit anti–β-actin (1:1,000 dilution for WB; 612656; BD), rabbit anti-FUS (1:100 for IF and 1:1,000 dilution for WB; 11570-1-AP; Protein Tech), rabbit anti-Hsp104 (1:1,000 for WB; ADI-SPA-1040-F; Enzo Life Science), mouse anti–α-tubulin (1:1,000 for IF and 1:4,000 dilution for WB; T6199; Sigma-Aldrich), rabbit anti–Glu-tubulin (1:250 for IF and 1:2,000 dilution for WB; ab48389; Abcam), mouse anti–Tyr-tubulin (1:1,000 for IF and 1:2,000 dilution for WB; T-9028; Sigma-Aldrich), rabbit anti-KIF3A (1:1,000 dilution for WB; ab11259; Abcam), goat anti-KIF5B #1 (1:100 for IF and 1:1,000 dilution for WB; EB05492; Everest Biotech), rabbit anti-KIF5B #2 (1:1,000 dilution for WB;

ab42492; Abcam), rabbit anti-KIF5C #1 (1:100 dilution for IF; GWB-MT519F; Genway Biotech Inc.), goat anti-KIF5C #2 (1:50 dilution for IF; sc-48607; Santa Cruz Biotechnology, Inc.), mouse anti–acetylated tubulin (1:5,000 for IF; T7451; Sigma-Aldrich), rabbit anti–phospho-eIF2α (1:100 for IF and 1:500 for WB; 9721S; Cell Signaling Technology), rabbit anti-eIF2α (1:1,000 for WB; 9722; Cell Signaling Technology), rabbit anti-GFP (1:1,000 for WB; A11122; Invitrogen), and mouse anti-GM130 (1:100 for IF; 610822; BD).

For WB, the following secondary antibodies were used: anti–rabbit (conjugated with IRDye 800CW; 1:15,000 dilution; 926-32213; LI-COR Biosciences; or conjugated with HRP; 1:1,000 dilution; R21459; Thermo Fisher Scientific), anti–mouse (conjugated with IRDye 680RD; 1:15,000 dilution; 926-68072; LI-COR Biosciences), and anti–goat (conjugated with IRDye 680RD; 1:15,000 dilution; 926-68074; LI-COR Biosciences). Membranes were scanned with Odyssey (LI-COR Biosciences) or were developed on film using the SuperSignal West Pico Chemiluminescent substrate (for total eIF2α; 34080; Thermo Fisher Scientific) or SuperSignal West Femto Maximum Sensitivity substrate (for phosphorylated eIF2α; 1:10 dilution; 34095, Thermo Fisher Scientific). Signal intensity was measured using Image Studio Lite software (LI-COR Biosciences) or Fiji (ImageJ; National Institutes of Health).

For IF, NIH/3T3 cells were plated onto micropatterned substrates or glass coverslips coated with fibronectin. Neurons were plated at 20,000 cells per 18-mm coverslip coated with poly-L-lysine. Cells were fixed with 4% PFA in PBS for 15 min at RT (or for 90 min at 4°C for Glu-tubulin staining), permeabilized with 0.2% Triton X-100 in PBS for 5 min (or with prechilled methanol for 5 min at −20°C for Glu-tubulin staining), blocked with 5% FBS for 1 h, and incubated with primary antibodies overnight at 4°C. Secondary antibodies were conjugated with Alexa Fluor 488, 546, or 647 (1:400 dilutions for each; Thermo Fisher Scientific). Nuclei were stained with DAPI. Samples were mounted on slide glass with Fluoromount-G (0100-01; SouthernBiotech). For nocodazole treatments depicted in Fig. 9 C, 5 µM nocodazole was added for the indicated times, and cells were permeabilized with digitonin (0.15 mg/ml for 4 min) before fixation and IF staining.

ER and mitochondria were fluorescently labeled by using ER Tracker Red (E34250) and MitoTracker Red (M7513; Thermo Fisher Scientific), respectively.

Image acquisition and analysis

IF images were obtained using either an LSM 510 or LSM 710 confocal microscope with ZEN software (ZEISS), a Leica SP8 confocal microscope with LASX software (equipped with either a high-contrast Plan-Apochromat 63× oil CS2 objective at 1.40 NA or a high-contrast Plan-Apochromat 40× oil CS2 objective at 1.30 NA; Leica Microsystems), or an EVOS FL microscope (equipped with a 40× Plan Coverslip Corrected FL Air objective at 0.75 NA; Thermo Fisher Scientific). For signal intensity measurements, all images were taken under the same settings, and signal intensity was measured on Fiji software after background subtraction.

FISH images were obtained using an LSM 510, LSM 710, or Leica SP8 confocal microscope. Edge ratio analysis was performed using Fiji. The channel detecting the cell mask stain was used to obtain a binary mask of the whole cell area. A filter was then applied to erode the mask by a specified number of pixels corresponding to 2 µm (or 0.5 µm where indicated), thus obtaining an inner cell mask. The two masks were used to measure signal intensity and area from background-subtracted FISH images. Values within the peripheral edge were obtained by subtracting the inner mask values from the whole-cell values. Using a semiautomated ImageJ macro, edge ratio was calculated as $(I_p/I_w)/(A_p/A_w)$, where I_p = FISH signal intensity in the peripheral edge, I_w = FISH signal intensity in the whole-cell mask, A_p = area of the peripheral edge, and A_w = area of the whole-cell mask.

Photobleaching was performed on an LSM 510 Meta confocal microscope. Temperature was maintained at 37°C. Medium pH was controlled by the addition of 25 mM Hepes buffer. Regions of interest were selected and bleached with the 488-nm argon laser line at 100% power and 100% transmission for two iterations. Fluorescence recovery within the region of interest was monitored for ∼60 s using the 488-nm laser line at 30% power and 5% transmission. For each experiment, three images were recorded prebleach. Mean intensities in the bleached area were measured, and background signal was subtracted. Background-subtracted intensities were further corrected for bleaching during imaging using measurements of an adjacent unbleached region and were expressed as a percentage of the prebleach intensity.

Online supplemental material

Fig. S1 shows FRAP experiments of GFP-FUS(R521C) inclusions and the effect of mutant FUS inclusions on stress response markers and on general cellular architecture. Fig. S2 shows the effect of mutant FUS inclusions on the distributions of *Kank2* and *Arpc3* RNAs and the effect of inclusions formed by the wild-type FUS protein. Fig. S3 shows changes in Glu-tubulin levels upon different treatments, validation of KIF5B and KIF5C antibody specificity, and the requirement of the IDR domain of KIF5B for accumulation in FUS inclusions. Fig. S4 shows the accumulation of YFP-KIF5B in FUS inclusions and the rescue of Ddr2 RNA localization upon overexpression of untagged KIF5B. It also shows a lack of accumulation of KIF5B in TDP-43(A315T) inclusions and a lack of rescue of RNA localization and Glu-MT structure upon YFP-KIF5B overexpression. Fig. S5 shows WB detection of TTL levels in knockdown experiments and IF quantitations of acetyl-tubulin levels in the presence or absence of FUS inclusions combined or uncombined with taxol treatment.

Acknowledgments

This work was supported by the Intramural Research Program of the Center for Cancer Research, National Cancer Institute, National Institutes of Health and a Japan Society for the Promotion of Science Fellowship to K. Yasuda; J. Shorter is supported by the National Institutes of Health grant R01GM099836, the Muscular Dystrophy Association Research Award (MDA277268), the Life Extension Foundation, the Packard Center for ALS Research at Johns Hopkins University, and Target ALS; M.E. Jackrel is supported by a Target ALS Springboard Fellowship.

The authors declare no competing financial interests.

Author contributions: Conceptualization, S. Mili and K. Yasuda; methodology, S. Mili and K. Yasuda; investigation, K. Yasuda and S. Mili; resources, M.E. Jackrel and J. Shorter; software, S.F. Clatterbuck-Soper; writing—original draft, S. Mili and K. Yasuda; writing—review and editing, S. Mili, K. Yasuda, and J. Shorter.

Submitted: 5 August 2016
Revised: 18 November 2016
Accepted: 19 January 2017

References

Alami, N.H., R.B. Smith, M.A. Carrasco, L.A. Williams, C.S. Winborn, S.S. Han, E. Kiskinis, B. Winborn, B.D. Freibaum, A. Kanagaraj, et al. 2014. Axonal transport of TDP-43 mRNA granules is impaired by ALS-causing mutations. *Neuron.* 81:536–543. http://dx.doi.org/10.1016/j.neuron.2013.12.018

Arce, C.A., and H.S. Barra. 1985. Release of C-terminal tyrosine from tubulin and microtubules at steady state. *Biochem. J.* 226:311–317. http://dx.doi.org/10.1042/bj2260311

Barisic, M., R. Silva e Sousa, S.K. Tripathy, M.M. Magiera, A.V. Zaytsev, A.L. Pereira, C. Janke, E.L. Grishchuk, and H. Maiato. 2015. Microtubule detyrosination guides chromosomes during mitosis. *Science.* 348:799–803. http://dx.doi.org/10.1126/science.aaa5175

Baron, D.M., L.J. Kaushansky, C.L. Ward, R.R. Sama, R.J. Chian, K.J. Boggio, A.J. Quaresma, J.A. Nickerson, and D.A. Bosco. 2013. Amyotrophic lateral sclerosis-linked FUS/TLS alters stress granule assembly and dynamics. *Mol. Neurodegener.* 8:30. http://dx.doi.org/10.1186/1750-1326-8-30

Barten, D.M., P. Fanara, C. Andorfer, N. Hoque, P.Y. Wong, K.H. Husted, G.W. Cadelina, L.B. Decarr, L. Yang, V. Liu, et al. 2012. Hyperdynamic microtubules, cognitive deficits, and pathology are improved in tau transgenic mice with low doses of the microtubule-stabilizing agent BMS-241027. *J. Neurosci.* 32:7137–7145. http://dx.doi.org/10.1523/JNEUROSCI.0188-12.2012

Blokhuis, A.M., E.J. Groen, M. Koppers, L.H. van den Berg, and R.J. Pasterkamp. 2013. Protein aggregation in amyotrophic lateral sclerosis. *Acta Neuropathol.* 125:777–794. http://dx.doi.org/10.1007/s00401-013-1125-6

Bosco, D.A., N. Lemay, H.K. Ko, H. Zhou, C. Burke, T.J. Kwiatkowski Jr., P. Sapp, D. McKenna-Yasek, R.H. Brown Jr., and L.J. Hayward. 2010. Mutant FUS proteins that cause amyotrophic lateral sclerosis incorporate into stress granules. *Hum. Mol. Genet.* 19:4160–4175. http://dx.doi.org/10.1093/hmg/ddq335

Brunden, K.R., J.Q. Trojanowski, A.B. Smith III, V.M. Lee, and C. Ballatore. 2014. Microtubule-stabilizing agents as potential therapeutics for neurodegenerative disease. *Bioorg. Med. Chem.* 22:5040–5049. http://dx.doi.org/10.1016/j.bmc.2013.12.046

Cai, D., D.P. McEwen, J.R. Martens, E. Meyhofer, and K.J. Verhey. 2009. Single molecule imaging reveals differences in microtubule track selection between kinesin motors. *PLoS Biol.* 7:e1000216. http://dx.doi.org/10.1371/journal.pbio.1000216

Courchaine, E.M., A. Lu, and K.M. Neugebauer. 2016. Droplet organelles? *EMBO J.* 35:1603–1612. http://dx.doi.org/10.15252/embj.201593517

Coyne, A.N., B.B. Siddegowda, P.S. Estes, J. Johannesmeyer, T. Kovalik, S.G. Daniel, A. Pearson, R. Bowser, and D.C. Zarnescu. 2014. Futsch/MAP1B mRNA is a translational target of TDP-43 and is neuroprotective in a *Drosophila* model of amyotrophic lateral sclerosis. *J. Neurosci.* 34:15962–15974. http://dx.doi.org/10.1523/JNEUROSCI.2526-14.2014

Coyne, A.N., S.B. Yamada, B.B. Siddegowda, P.S. Estes, B.L. Zaepfel, J.S. Johannesmeyer, D.B. Lockwood, L.T. Pham, M.P. Hart, J.A. Cassel, et al. 2015. Fragile X protein mitigates TDP-43 toxicity by remodeling RNA granules and restoring translation. *Hum. Mol. Genet.* 24:6886–6898.

Di Giovanni, S., C.D. Knights, M. Rao, A. Yakovlev, J. Beers, J. Catania, M.L. Avantaggiati, and A.I. Faden. 2006. The tumor suppressor protein p53 is required for neurite outgrowth and axon regeneration. *EMBO J.* 25:4084–4096. http://dx.doi.org/10.1038/sj.emboj.7601292

Dini Modigliani, S., M. Morlando, L. Errichelli, M. Sabatelli, and I. Bozzoni. 2014. An ALS-associated mutation in the FUS 3′-UTR disrupts a microRNA-FUS regulatory circuitry. *Nat. Commun.* 5:4335. http://dx.doi.org/10.1038/ncomms5335

Dormann, D., R. Rodde, D. Edbauer, E. Bentmann, I. Fischer, A. Hruscha, M.E. Than, I.R. Mackenzie, A. Capell, B. Schmid, et al. 2010. ALS-associated fused in sarcoma (*FUS*) mutations disrupt Transportin-mediated nuclear import. *EMBO J.* 29:2841–2857. http://dx.doi.org/10.1038/emboj.2010.143

Dunn, S., E.E. Morrison, T.B. Liverpool, C. Molina-París, R.A. Cross, M.C. Alonso, and M. Peckham. 2008. Differential trafficking of Kif5c on tyrosinated and detyrosinated microtubules in live cells. *J. Cell Sci.* 121:1085–1095. http://dx.doi.org/10.1242/jcs.026492

Fanara, P., J. Banerjee, R.V. Hueck, M.R. Harper, M. Awada, H. Turner, K.H. Husted, R. Brandt, and M.K. Hellerstein. 2007. Stabilization of hyperdynamic microtubules is neuroprotective in amyotrophic lateral sclerosis. *J. Biol. Chem.* 282:23465–23472. http://dx.doi.org/10.1074/jbc.M703434200

Fonrose, X., F. Ausseil, E. Soleilhac, V. Masson, B. David, I. Pouny, J.C. Cintrat, B. Rousseau, C. Barette, G. Massiot, and L. Lafanechère. 2007. Parthenolide inhibits tubulin carboxypeptidase activity. *Cancer Res.* 67:3371–3378. http://dx.doi.org/10.1158/0008-5472.CAN-06-3732

Hammond, J.W., D. Cai, and K.J. Verhey. 2008. Tubulin modifications and their cellular functions. *Curr. Opin. Cell Biol.* 20:71–76. http://dx.doi.org/10.1016/j.ceb.2007.11.010

Herms, A., M. Bosch, B.J. Reddy, N.L. Schieber, A. Fajardo, C. Rupérez, A. Fernández-Vidal, C. Ferguson, C. Rentero, F. Tebar, et al. 2015. AMPK activation promotes lipid droplet dispersion on detyrosinated microtubules to increase mitochondrial fatty acid oxidation. *Nat. Commun.* 6:7176. http://dx.doi.org/10.1038/ncomms8176

Hoell, J.I., E. Larsson, S. Runge, J.D. Nusbaum, S. Duggimpudi, T.A. Farazi, M. Hafner, A. Borkhardt, C. Sander, and T. Tuschl. 2011. RNA targets of wild-type and mutant FET family proteins. *Nat. Struct. Mol. Biol.* 18:1428–1431. http://dx.doi.org/10.1038/nsmb.2163

Ishigaki, S., A. Masuda, Y. Fujioka, Y. Iguchi, M. Katsuno, A. Shibata, F. Urano, G. Sobue, and K. Ohno. 2012. Position-dependent FUS-RNA interactions regulate alternative splicing events and transcriptions. *Sci. Rep.* 2:529. http://dx.doi.org/10.1038/srep00529

Jackrel, M.E., and J. Shorter. 2014. Potentiated Hsp104 variants suppress toxicity of diverse neurodegenerative disease-linked proteins. *Dis. Model. Mech.* 7:1175–1184. http://dx.doi.org/10.1242/dmm.016113

Jackrel, M.E., M.E. DeSantis, B.A. Martinez, L.M. Castellano, R.M. Stewart, K.A. Caldwell, G.A. Caldwell, and J. Shorter. 2014. Potentiated Hsp104 variants antagonize diverse proteotoxic misfolding events. *Cell.* 156:170–182. http://dx.doi.org/10.1016/j.cell.2013.11.047

Jain, S., J.R. Wheeler, R.W. Walters, A. Agrawal, A. Barsic, and R. Parker. 2016. ATPase-modulated stress granules contain a diverse proteome and substructure. *Cell.* 164:487–498. http://dx.doi.org/10.1016/j.cell.2015.12.038

Janke, C. 2014. The tubulin code: molecular components, readout mechanisms, and functions. *J. Cell Biol.* 206:461–472. http://dx.doi.org/10.1083/jcb.201406055

Jaulin, F., and G. Kreitzer. 2010. KIF17 stabilizes microtubules and contributes to epithelial morphogenesis by acting at MT plus ends with EB1 and APC. *J. Cell Biol.* 190:443–460. http://dx.doi.org/10.1083/jcb.201006044

Jung, H., B.C. Yoon, and C.E. Holt. 2012. Axonal mRNA localization and local protein synthesis in nervous system assembly, maintenance and repair. *Nat. Rev. Neurosci.* 13:308–324. http://dx.doi.org/10.1038/nrn3274

Kanai, Y., N. Dohmae, and N. Hirokawa. 2004. Kinesin transports RNA: isolation and characterization of an RNA-transporting granule. *Neuron.* 43:513–525. http://dx.doi.org/10.1016/j.neuron.2004.07.022

Kato, M., T.W. Han, S. Xie, K. Shi, X. Du, L.C. Wu, H. Mirzaei, E.J. Goldsmith, J. Longgood, J. Pei, et al. 2012. Cell-free formation of RNA granules: low complexity sequence domains form dynamic fibers within hydrogels. *Cell.* 149:753–767. http://dx.doi.org/10.1016/j.cell.2012.04.017

King, O.D., A.D. Gitler, and J. Shorter. 2012. The tip of the iceberg: RNA-binding proteins with prion-like domains in neurodegenerative disease. *Brain Res.* 1462:61–80. http://dx.doi.org/10.1016/j.brainres.2012.01.016

Konishi, Y., and M. Setou. 2009. Tubulin tyrosination navigates the kinesin-1 motor domain to axons. *Nat. Neurosci.* 12:559–567. http://dx.doi.org/10.1038/nn.2314

Kumar, N., and M. Flavin. 1981. Preferential action of a brain detyrosinolating carboxypeptidase on polymerized tubulin. *J. Biol. Chem.* 256:7678–7686.

Kwiatkowski, T.J. Jr., D.A. Bosco, A.L. Leclerc, E. Tamrazian, C.R. Vanderburg, C. Russ, A. Davis, J. Gilchrist, E.J. Kasarskis, T. Munsat, et al. 2009. Mutations in the *FUS/TLS* gene on chromosome 16 cause familial amyotrophic lateral sclerosis. *Science.* 323:1205–1208. http://dx.doi.org/10.1126/science.1166066

Lagier-Tourenne, C., M. Polymenidou, and D.W. Cleveland. 2010. TDP-43 and FUS/TLS: emerging roles in RNA processing and neurodegeneration. *Hum. Mol. Genet.* 19(R1):R46–R64. http://dx.doi.org/10.1093/hmg/ddq137

Li, Y.R., O.D. King, J. Shorter, and A.D. Gitler. 2013. Stress granules as crucibles of ALS pathogenesis. *J. Cell Biol.* 201:361–372. http://dx.doi.org/10.1083/jcb.201302044

Lin, Y., D.S. Protter, M.K. Rosen, and R. Parker. 2015. Formation and maturation of phase-separated liquid droplets by RNA-binding proteins. *Mol. Cell.* 60:208–219. http://dx.doi.org/10.1016/j.molcel.2015.08.018

Ling, S.C., M. Polymenidou, and D.W. Cleveland. 2013. Converging mechanisms in ALS and FTD: disrupted RNA and protein homeostasis. *Neuron.* 79:416–438. http://dx.doi.org/10.1016/j.neuron.2013.07.033

Liu-Yesucevitz, L., A. Bilgutay, Y.J. Zhang, T. Vanderweyde, A. Citro, T. Mehta, N. Zaarur, A. McKee, R. Bowser, M. Sherman, et al. 2010. Tar DNA binding protein-43 (TDP-43) associates with stress granules: analysis of cultured cells and pathological brain tissue. *PLoS One.* 5:e13250 (published erratum appears in *PLoS One*. 2011. 6). https://doi.org/10.1371/journal.pone.0013250

Liu-Yesucevitz, L., G.J. Bassell, A.D. Gitler, A.C. Hart, E. Klann, J.D. Richter, S.T. Warren, and B. Wolozin. 2011. Local RNA translation at the synapse and in disease. *J. Neurosci.* 31:16086–16093. http://dx.doi.org/10.1523/JNEUROSCI.4105-11.2011

Loschi, M., C.C. Leishman, N. Berardone, and G.L. Boccaccio. 2009. Dynein and kinesin regulate stress-granule and P-body dynamics. *J. Cell Sci.* 122:3973–3982. http://dx.doi.org/10.1242/jcs.051383

Mili, S., K. Moissoglu, and I.G. Macara. 2008. Genome-wide screen reveals APC-associated RNAs enriched in cell protrusions. *Nature.* 453:115–119. http://dx.doi.org/10.1038/nature06888

Molliex, A., J. Temirov, J. Lee, M. Coughlin, A.P. Kanagaraj, H.J. Kim, T. Mittag, and J.P. Taylor. 2015. Phase separation by low complexity domains promotes stress granule assembly and drives pathological fibrillization. *Cell.* 163:123–133. http://dx.doi.org/10.1016/j.cell.2015.09.015

Morris, E.J., G.P. Nader, N. Ramalingam, F. Bartolini, and G.G. Gundersen. 2014. Kif4 interacts with EB1 and stabilizes microtubules downstream of Rho-mDia in migrating fibroblasts. *PLoS One.* 9:e91568. http://dx.doi.org/10.1371/journal.pone.0091568

Murakami, T., S. Qamar, J.Q. Lin, G.S. Schierle, E. Rees, A. Miyashita, A.R. Costa, R.B. Dodd, F.T. Chan, C.H. Michel, et al. 2015. ALS/FTD mutation-induced phase transition of FUS liquid droplets and reversible hydrogels into irreversible hydrogels impairs RNP granule function. *Neuron.* 88:678–690. http://dx.doi.org/10.1016/j.neuron.2015.10.030

Nakaya, T., P. Alexiou, M. Maragkakis, A. Chang, and Z. Mourelatos. 2013. FUS regulates genes coding for RNA-binding proteins in neurons by binding to their highly conserved introns. *RNA.* 19:498–509. http://dx.doi.org/10.1261/rna.037804.112

Nijholt, D.A., E.S. van Haastert, A.J. Rozemuller, W. Scheper, and J.J. Hoozemans. 2012. The unfolded protein response is associated with early tau pathology in the hippocampus of tauopathies. *J. Pathol.* 226:693–702. http://dx.doi.org/10.1002/path.3969

Patel, A., H.O. Lee, L. Jawerth, S. Maharana, M. Jahnel, M.Y. Hein, S. Stoynov, J. Mahamid, S. Saha, T.M. Franzmann, et al. 2015. A liquid-to-solid phase transition of the ALS protein FUS accelerated by disease mutation. *Cell.* 162:1066–1077. http://dx.doi.org/10.1016/j.cell.2015.07.047

Preitner, N., J. Quan, D.W. Nowakowski, M.L. Hancock, J. Shi, J. Tcherkezian, T.L. Young-Pearse, and J.G. Flanagan. 2014. APC is an RNA-binding protein, and its interactome provides a link to neural development and microtubule assembly. *Cell.* 158:368–382. http://dx.doi.org/10.1016/j.cell.2014.05.042

Prota, A.E., M.M. Magiera, M. Kuijpers, K. Bargsten, D. Frey, M. Wieser, R. Jaussi, C.C. Hoogenraad, R.A. Kammerer, C. Janke, and M.O. Steinmetz. 2013. Structural basis of tubulin tyrosination by tubulin tyrosine ligase. *J. Cell Biol.* 200:259–270. http://dx.doi.org/10.1083/jcb.201211017

Protter, D.S., and R. Parker. 2016. Principles and properties of stress granules. *Trends Cell Biol.* 26:668–679. http://dx.doi.org/10.1016/j.tcb.2016.05.004

Ramaswami, M., J.P. Taylor, and R. Parker. 2013. Altered ribostasis: RNA-protein granules in degenerative disorders. *Cell.* 154:727–736. http://dx.doi.org/10.1016/j.cell.2013.07.038

Renton, A.E., A. Chiò, and B.J. Traynor. 2014. State of play in amyotrophic lateral sclerosis genetics. *Nat. Neurosci.* 17:17–23. http://dx.doi.org/10.1038/nn.3584

Rivera, J., P.J. Chu, T.L. Lewis Jr., and D.B. Arnold. 2007. The role of Kif5B in axonal localization of Kv1 K^+ channels. *Eur. J. Neurosci.* 25:136–146. http://dx.doi.org/10.1111/j.1460-9568.2006.05277.x

Rogelj, B., L.E. Easton, G.K. Bogu, L.W. Stanton, G. Rot, T. Curk, B. Zupan, Y. Sugimoto, M. Modic, N. Haberman, et al. 2012. Widespread binding of FUS along nascent RNA regulates alternative splicing in the brain. *Sci. Rep.* 2:603. http://dx.doi.org/10.1038/srep00603

Ruane, P.T., L.F. Gumy, B. Bola, B. Anderson, M.J. Wozniak, C.C. Hoogenraad, and V.J. Allan. 2016. Tumour suppressor adenomatous polyposis coli (APC) localisation is regulated by both Kinesin-1 and Kinesin-2. *Sci. Rep.* 6:27456. http://dx.doi.org/10.1038/srep27456

Sabatelli, M., A. Moncada, A. Conte, S. Lattante, G. Marangi, M. Luigetti, M. Lucchini, M. Mirabella, A. Romano, A. Del Grande, et al. 2013. Mutations in the 3′ untranslated region of *FUS* causing FUS overexpression are associated with amyotrophic lateral sclerosis. *Hum. Mol. Genet.* 22:4748–4755.

Seeger, M.A., and S.E. Rice. 2013. Intrinsic disorder in the kinesin superfamily. *Biophys. Rev.* 5:233. http://dx.doi.org/10.1007/s12551-012-0096-5

Shelkovnikova, T.A. 2013. Modelling FUSopathies: focus on protein aggregation. *Biochem. Soc. Trans.* 41:1613–1617. http://dx.doi.org/10.1042/BST20130212

Smith, B.N., N. Ticozzi, C. Fallini, A.S. Gkazi, S. Topp, K.P. Kenna, E.L. Scotter, J. Kost, P. Keagle, J.W. Miller, et al. SLAGEN Consortium. 2014. Exome-wide rare variant analysis identifies TUBA4A mutations associated with familial ALS. *Neuron.* 84:324–331. http://dx.doi.org/10.1016/j.neuron.2014.09.027

Sun, Z., Z. Diaz, X. Fang, M.P. Hart, A. Chesi, J. Shorter, and A.D. Gitler. 2011. Molecular determinants and genetic modifiers of aggregation and toxicity for the ALS disease protein FUS/TLS. *PLoS Biol.* 9:e1000614. http://dx.doi.org/10.1371/journal.pbio.1000614

Szyk, A., G. Piszczek, and A. Roll-Mecak. 2013. Tubulin tyrosine ligase and stathmin compete for tubulin binding *in vitro*. *J. Mol. Biol.* 425:2412–2414. http://dx.doi.org/10.1016/j.jmb.2013.04.017

Tan, A.Y., and J.L. Manley. 2009. The TET family of proteins: functions and roles in disease. *J. Mol. Cell Biol.* 1:82–92. http://dx.doi.org/10.1093/jmcb/mjp025

Vance, C., E.L. Scotter, A.L. Nishimura, C. Troakes, J.C. Mitchell, C. Kathe, H. Urwin, C. Manser, C.C. Miller, T. Hortobágyi, et al. 2013. ALS mutant FUS disrupts nuclear localization and sequesters wild-type FUS within cytoplasmic stress granules. *Hum. Mol. Genet.* 22:2676–2688. http://dx.doi.org/10.1093/hmg/ddt117

van Schadewijk, A., E.F. van't Wout, J. Stolk, and P.S. Hiemstra. 2012. A quantitative method for detection of spliced X-box binding protein-1 (XBP1) mRNA as a measure of endoplasmic reticulum (ER) stress. *Cell Stress Chaperones.* 17:275–279. http://dx.doi.org/10.1007/s12192-011-0306-2

Weber, S.C., and C.P. Brangwynne. 2012. Getting RNA and protein in phase. *Cell.* 149:1188–1191. http://dx.doi.org/10.1016/j.cell.2012.05.022

Wehland, J., and K. Weber. 1987. Turnover of the carboxy-terminal tyrosine of alpha-tubulin and means of reaching elevated levels of detyrosination in living cells. *J. Cell Sci.* 88:185–203.

Wheeler, J.R., T. Matheny, S. Jain, R. Abrisch, and R. Parker. 2016. Distinct stages in stress granule assembly and disassembly. *eLife.* 5:e18413. http://dx.doi.org/10.7554/eLife.18413

Yasuda, K., and S. Mili. 2016. Dysregulated axonal RNA translation in amyotrophic lateral sclerosis. *Wiley Interdiscip. Rev. RNA.* 7:589–603. http://dx.doi.org/10.1002/wrna.1352

Yasuda, K., H. Zhang, D. Loiselle, T. Haystead, I.G. Macara, and S. Mili. 2013. The RNA-binding protein Fus directs translation of localized mRNAs in APC-RNP granules. *J. Cell Biol.* 203:737–746. http://dx.doi.org/10.1083/jcb.201306058

Yoshiyama, Y., B. Zhang, J. Bruce, J.Q. Trojanowski, and V.M. Lee. 2003. Reduction of detyrosinated microtubules and Golgi fragmentation are linked to tau-induced degeneration in astrocytes. *J. Neurosci.* 23:10662–10671.

Zhang, B., A. Maiti, S. Shively, F. Lakhani, G. McDonald-Jones, J. Bruce, E.B. Lee, S.X. Xie, S. Joyce, C. Li, et al. 2005. Microtubule-binding drugs offset tau sequestration by stabilizing microtubules and reversing fast axonal transport deficits in a tauopathy model. *Proc. Natl. Acad. Sci. USA.* 102:227–231. http://dx.doi.org/10.1073/pnas.0406361102